AGU Advances

RESEARCH ARTICLE
10.1029/2019AV000159

Key Points:
- Neoproterozoic preglacial and glacial carbonates preserve differences in $\delta^{18}O$ and carbonate clumped isotope temperatures
- A population of synglacial dolostones yield mean Δ_{47} temperatures 26 ± 10 °C (95% CL) cooler than lithified preglacial dolostones
- Clumped isotope temperatures <25°C ($n = 4$) bolster confidence in a depositional or early diagenetic source for the $\delta^{18}O$ isotopic record

Supporting Information:
- Supporting Information S1
- Original Version of Manuscript
- Peer Review History
- First Revision of Manuscript
- Author Response to Peer Review Comments
- Second Revision of Manuscript [Accepted]
- Author Response to Peer Review Comments

Correspondence to:
T. J. Mackey,
tjmackey@unm.edu

Citation:
Mackey, T. J., Jost, A. B., Creveling, J. R., & Bergmann, K. D. (2020). A decrease to low carbonate clumped isotope temperatures in Cryogenian strata. *AGU Advances*, *1*, e2019AV000159. https://doi.org/10.1029/2019AV000159

Received 20 DEC 2019
Accepted 9 JUN 2020

Peer Review The peer review history for this article is available as a PDF in the Supporting Information.

Author Contributions:
Conceptualization: K. D. Bergmann
Investigation: T. J. Mackey
Methodology: A. B. Jost
(continued)

©2020. The Authors.
This is an open access article under the terms of the Creative Commons Attribution License, which permits use, distribution and reproduction in any medium, provided the original work is properly cited.

A Decrease to Low Carbonate Clumped Isotope Temperatures in Cryogenian Strata

T. J. Mackey[1,2], A. B. Jost[1], J. R. Creveling[3], and K. D. Bergmann[1]

[1]Department of Earth, Atmospheric, and Planetary Sciences, Massachusetts Institute of Technology, Cambridge, MA, USA, [2]Now at Department of Earth and Planetary Sciences, University of New Mexico, Albuquerque, NM, USA, [3]College of Earth, Ocean, and Atmospheric Sciences, Oregon State University, Corvallis, OR, USA

Abstract Preglacial and synglacial low-latitude carbonate sediments of the Elbobreen Formation, NE Svalbard, preserve facies changes associated with low-latitude glacial advance in Cryogenian "Snowball Earth" episodes (717–635 Ma). We present the first application of carbonate clumped (Δ_{47}) isotope thermometry on synglacial Snowball Earth carbonates and combine results with sedimentologic and petrographic observations and stable isotope ($\delta^{13}C$ and $\delta^{18}O$) geochemistry to assess Neoproterozoic environmental change. We find elevated calcite Δ_{47} temperatures, which likely reflect solid-state reordering during burial. Dolomites, however, record lower temperatures that vary with facies and stratigraphy. Preglacial dolomite Δ_{47} temperatures range from 48–77°C, with a reconstructed fluid $\delta^{18}O_{VSMOW}$ value of +0.6‰ in the coldest sample. Glacial diamictites and dolomicrites comprise (1) reworked detrital clasts similar to preglacial strata in stable isotope composition and petrographic textures and (2) autochthonous dolomicrite with more positive $\delta^{18}O$ values than those of preglacial dolomites or cooccurring detrital clasts. Mean glacial autochthonous dolomicrite Δ_{47} temperatures are 26 ± 10°C (95% CL) cooler than preglacial strata, with four samples <25°C. All dolomite Δ_{47} temperatures reflect diagenesis associated with lithification, yet observed stratigraphic and textural Δ_{47} temperature differences indicate that this occurred early and only contributes to part of the preserved temperature signal. Alteration trends within populations are consistent with low water/rock ratio diagenesis or partial solid-state reordering; either possibility supports the likelihood of preserved $\delta^{18}O$ trends. We postulate that the preserved temperature and $\delta^{18}O$ differences between low-latitude preglacial Tonian and synglacial Cryogenian dolomites are an imperfect reflection of primary temperature change and ice sheet expansion.

Plain Language Summary Glaciations, termed "Snowball Earth" episodes, with evidence for low-latitude ice took place in the Cryogenian (717–635 Ma), and these extreme glaciations were likely a critical part of the transition between the Precambrian and the Phanerozoic (541 Ma to present). In this study, we analyzed strata from Svalbard that were originally deposited near the equator before and during one of these Snowball Earth events and present the first application of carbonate clumped isotope (Δ_{47}) thermometry to Cryogenian synglacial deposits. We combine Δ_{47} results with both $^{18}O/^{16}O$ stable isotope composition of the carbonates and their microscopic character to assess evidence for environmental changes associated with this glaciation. Carbonates maintain a record of significantly (20–30°C) lower Δ_{47} temperatures in glacial versus preglacial deposits. Carbonate $^{18}O/^{16}O$ enrichment in synglacial deposits is consistent with ice sheet expansion in the Cryogenian. If the observed drop in temperature from preglacial to glacial strata reflects a difference in primary or shallow pore fluid temperatures, it far exceeds that of more recent Phanerozoic glaciations like the Pleistocene.

1. Introduction

Earth's Phanerozoic climate was dominated by "greenhouse" conditions without polar ice, with brief forays into "icehouse" states similar to today (Brenchley et al., 1994; Montañez & Poulsen, 2013). Prior to the Phanerozoic Eon, low-latitude, Neoproterozoic glacial deposits provide evidence of a third, panglacial climate state colloquially referred to as a "Snowball Earth" (Hoffman, 2009; Hoffman et al., 1998; Kirschvink, 1992). Snowball Earth episodes are thought to represent a positive feedback between ice cover and albedo with expansion of sea ice to low latitudes, until volcanic outgassing and greenhouse warming overcomes albedo (Hoffman et al., 1998). Accordingly, the Snowball Earth hypothesis predicts that the onset and termination of low-latitude glaciation was globally synchronous (Kirschvink, 1992). Recent radiometric

Resources: T. J. Mackey, A. B. Jost, J. R. Creveling, K. D. Bergmann
Supervision: K. D. Bergmann
Visualization: K. D. Bergmann
Writing - original draft: T. J. Mackey
Writing – review & editing: T. J. Mackey, A. B. Jost, J. R. Creveling, K. D. Bergmann

constraints have confirmed the synchronous initiation and termination of Neoproterozoic glaciations within the uncertainty of analyses (Macdonald et al., 2010; Rooney et al., 2015). This revised chronology indicates the earlier of the two Neoproterozoic Snowball glaciations lasted at least 57 Ma (Hoffman et al., 2017; Macdonald et al., 2010; Rooney et al., 2015), requiring climate dynamics distinct from subsequent Phanerozoic glaciations (e.g., Abbot et al., 2013; Ewing et al., 2014; Hyde et al., 2000; Yang et al., 2017).

Carbonate rocks provide an archive of Earth's past climate states. Carbonate δ^{18}O values are a product of source fluid δ^{18}O values and a temperature-dependent fractionation factor (S.-T. Kim & O'Neil, 1997; Urey, 1948), thus providing a measure of seawater δ^{18}O values where temperature is known and vice versa. Recent Phanerozoic climate reconstructions are informed by combining the δ^{18}O values of sedimentary carbonates with independent temperature estimates (e.g., Δ_{47}, Mg/Ca ratios, and TEX86; Eggins et al., 2003; Ghosh et al., 2006; J. H. Kim et al., 2008; Finnegan et al., 2011; Evans et al., 2018). These combined records provide a powerful tool to assess changes in temperature, glacial hydrology, and ice sheet expansion. Evaporative export of marine water to continental ice sheets increased marine water δ^{18}O values during Phanerozoic glacial-interglacial cycles (Shackleton, 1967), with marine water $\delta^{18}O_{VSMOW}$ values approximately 2–3‰ higher in Pleistocene glaciations over estimated ice-free marine values of −1.2‰ (Cramer et al., 2011; Lea et al., 2000; Lear et al., 2000). This trend holds for estimates of seawater enrichment for the most recent glacial-interglacial transitions (Raymo et al., 2018), as well as earlier glacial episodes of the Late Paleozoic Ice Age (Grossman et al., 2008) and the end-Ordovician glaciation (Finnegan et al., 2011).

Climate signals preserved in carbonate δ^{18}O can be altered by fluids throughout diagenesis (e.g., Knauth & Kennedy, 2009; Swart & Kennedy, 2012); primary δ^{18}O values are diluted by incorporation of cements during lithification or erased by dissolution and reprecipitation (Dickson & Coleman, 1980; Huntington et al., 2011; Lohmann, 1988; Winkelstern & Lohmann, 2016). Application of carbonate δ^{18}O as a thermometer within Paleozoic and older carbonates is further complicated by uncertainty in seawater δ^{18}O values (e.g., Jaffrés et al., 2007). This uncertainty yields a wide range in temperature estimates through the Paleozoic and Neoproterozoic (Henkes et al., 2017; Jean-Baptiste et al., 1997; Kasting et al., 2006; Veizer et al., 1999).

Recent reconstructions of Paleozoic and Ediacaran seawater δ^{18}O values have leveraged the carbonate clumped isotope thermometer (section 1.1) to independently calculate the temperature of carbonate precipitation. The clumped isotope system of carbonate rocks is always affected by lithification and is highly sensitive to further effects of postdepositional alteration; preservation of climatically relevant information in deep time accordingly requires early lithification and low maximum burial temperatures (Henkes et al., 2018; Passey & Henkes, 2012; Stolper & Eiler, 2015). In exceptionally preserved strata, this approach has informed interpretation of the traditional carbonate δ^{18}O thermometer, with broadly consistent seawater δ^{18}O values through the early Paleozoic and Ediacaran (Bergmann, al Balushi, et al., 2018; Bergmann, Finnegan, et al., 2018; Henkes et al., 2018). Extending the clumped isotope thermometer to assess the carbonate record of climate in Neoproterozoic Snowball Earth episodes requires the coincidence of a well-defined stratigraphic record of carbonates across climate states and subsequent shallow burial history. The Elbobreen Formation of NE Svalbard (section 1.2) likely records one instance of strata suitable for clumped isotope interrogation of carbonates across climate states.

In this study, we present a novel application of carbonate clumped isotope thermometry to pre-Snowball and syn-Snowball Earth glacial carbonates and assess the preservation of environmental signatures through the first of the Neoproterozoic glaciations. If early lithification signatures of carbonate δ^{18}O can be identified through the Neoproterozoic, the carbonate record may be able refine Snowball Earth climate models with constraints on preglacial, synglacial, and postglacial changes in temperature and ice volume (e.g., Benn et al., 2015; Creveling & Mitrovica, 2014).

1.1. Carbonate Clumped Isotope Analysis

Carbonate clumped isotope thermometry provides a potential means to explore the carbonate δ^{18}O record by independently measuring the temperature of carbonate precipitation. This thermometer is based on the temperature-dependent clumping of ^{13}C and ^{18}O into multiply substituted carbonate isotopologues (Δ_{47}; Eiler, 2007), and multiple carbonate mineralogies generally have similar temperature dependencies (Bonifacie et al., 2017; Bergmann, Finnegan, et al., 2018; see Bonifacie et al., 2017; Petersen et al., 2019;

Müller et al., 2019, for discussion of dolomite calibrations). Refinement of the technique has led to consistent interlaboratory calibrations across a range of instrumental configurations (Bernasconi et al., 2018; Fernandez et al., 2017; Kelson et al., 2017; Petersen et al., 2019). Δ_{47} temperatures can be combined with the mineral $\delta^{18}O$ values to calculate the $\delta^{18}O$ carbonate source fluid values, given the water-carbonate $^{18}O/^{16}O$ fractionation factors for a given carbonate mineralogy (e.g., calcite, S.-T. Kim & O'Neil, 1997; dolomite, Horita, 2008).

Application of the carbonate clumped isotope thermometer to the sedimentary record is complicated by the susceptibility of Δ_{47} values to alteration during diagenesis and burial. Processes including dissolution and reprecipitation or changes in mineralogy like dolomitization will move Δ_{47} temperatures toward the local geothermal gradient (Bergmann, al Balushi, et al., 2018; Ryb & Eiler, 2018; Staudigel & Swart, 2019; Winkelstern & Lohmann, 2016). Similarly, postdepositional cementation of primary grains dilutes clumped isotope signatures with carbonate material that is equilibrated to burial temperatures (Mangenot et al., 2018). Thus, both the extent of alteration (itself a function of primary grain size, porosity and mineralogy; e.g., Bergmann, al Balushi, et al., 2018; Staudigel & Swart, 2019) and the burial depth at which alteration takes place (Stolper et al., 2018) determine the magnitude of diagenetic change in Δ_{47} temperature. Such processes can be variably fluid or rock buffered and affect carbonate $\delta^{18}O$ values differently (e.g., Eiler, 2011), leading to populations of $\delta^{18}O$ values and Δ_{47} temperatures that covary with the diagenetic history (Bergmann, al Balushi, et al., 2018). If strata experience fluid-buffered diagenesis, carbonates will approach mineral $\delta^{18}O$ values in equilibrium with the diagenetic fluids for that burial temperature (e.g., Huntington et al., 2011; Mangenot et al., 2018). In contrast, carbonates experiencing rock-buffered diagenesis can have increased Δ_{47} temperatures without concomitant changes in mineral $\delta^{18}O$ values (Bergmann, al Balushi, et al., 2018; Cummins et al., 2014; Lacroix & Niemi, 2019; Staudigel & Swart, 2019). It is possible to assess the timing and extent of such alteration processes through comparison of Δ_{47} temperatures with carbonate petrographic indications of cementation, dissolution, and reprecipitation and independent estimates of thermal history (Bergmann, al Balushi, et al., 2018; Gilbert et al., 2017; Mangenot et al., 2018).

Carbonate clumped isotope records can be further altered by solid-state reordering. Solid-state reordering is the reequilibration of individual multiply substituted isotopologues within a carbonate mineral at elevated temperature (Henkes et al., 2014; Passey & Henkes, 2012; Stolper & Eiler, 2015); this process leads to resetting of clumped isotope temperatures associated with carbonate precipitation to fully or partially reflect elevated burial temperatures. Models for this reordering explain experimental observations of reordering kinetics by either (1) the diffusive propagation of defects (Henkes et al., 2014; Passey & Henkes, 2012) or (2) a two-step reaction between adjacent carbonate molecules and then successive diffusion through the carbonate crystal lattice (Stolper & Eiler, 2015). The kinetics of reordering over geologic time scales is temperature dependent, and this relationship has been shown to vary by carbonate mineralogy. Reordering experiments and supporting field studies of carbonate strata indicate that calcite reorders at temperatures above ~100°C over 10^6 to 10^8 years (Henkes et al., 2014), whereas dolomite begins to partially reorder above ~150°C over $>10^7$ years (Lloyd et al., 2018). Experimental and empirical observations are limited for carbonates experiencing moderate temperatures (50–150°C) over long time periods relevant to the Neoproterozoic, but some strata with burial temperatures below the threshold for solid-state reordering maintain low temperatures consistent with early lithification or diagenesis over $>10^8$ years (Bergmann, al Balushi, et al., 2018; Cummins et al., 2014; Finnegan et al., 2011; Henkes et al., 2018).

The Cryogenian glacial carbonates investigated in this study provide a test case for the preservation of clumped isotope signatures in micritic carbonates over longer time scales. Given the sensitivity of the carbonate clumped isotope system to modification via lithification and alteration during shallow burial and solid-state reordering during deeper burial, any attempt to assess changes in climate using this thermometer must first characterize evidence for solid-state reordering as well as both diagenetic alteration and timing of lithification and subsequent crystallization events. Our samples include both calcites and early fabric-retentive dolomites, and because of the different susceptibility of these minerals to solid-state reordering (Henkes et al., 2014; Lloyd et al., 2018; Stolper & Eiler, 2015), their respective clumped isotope temperatures can be used to estimate maximum burial temperature and to constrain the extent of solid-state reordering. In addition, the combined use of petrography and the style of clumped isotope alteration within a coherent population of genetically linked carbonates offers a means of identifying fluid versus

rock-buffered diagenesis and provides insights on how to interpret carbonate $\delta^{18}O$ values (Bergmann, al Balushi, et al., 2018).

1.2. Geologic Setting

Strata from NE Svalbard investigated in this study consist of mixed siliciclastic and carbonate rocks originally deposited in a long-lived basin at low paleolatitudes (Fairchild et al., 1989; Hoffman et al., 2012; Maloof et al., 2006). Neoproterozoic-Ordovician strata have been divided into the Veteranan, Akademikerbreen, Polarisbreen, and Oslobreen groups, and key sections are presently exposed along a 180 km belt across northeast Olav V Land, Ny Friesland, and west Nordaustlandet (Fairchild et al., 1989; Halverson et al., 2004; Harland et al., 1966) (Figure 1).

While absolute age constraints are lacking, based on a variety of observations, the onset of Cryogenian glaciation is thought to be preserved in the transition between the Russøya and Petrovbreen members of the Elbobreen Formation in the Polarisbreen Group (Fairchild et al., 1989; Halverson et al., 2018). These members contain abundant carbonate and are the focus of this study. Regionally, the Russøya Member begins with a transgression over peritidal facies of the Kinnvika Member (Dartboard Dolomite) in the Backlundtoppen Formation of the Akademikerbreen Group (Halverson et al., 2018). This transgression reflects the start of two marine transgressive-regressive sequences in the Russøya Member (T-R7 and 8 of Halverson et al., 2004, 2018). Lower transgressive Russøya Member strata are composed of calcite but transition to dolomite up section (Halverson et al., 2004, 2018). The overlying Petrovbreen Member varies in thickness across NE Svalbard, with the thickest sections exceeding 50 m in Ny Friesland. These strata include dolomitic rhythmite, wackestone, and siltstone containing outsized clasts interpreted as glacial dropstones, and diamictite with siliciclastic or dolomicrite matrix (Fairchild & Hambrey, 1984; Fairchild et al., 1989; Halverson et al., 2004). Facies are interpreted as marine or glaciolacustrine depositional environments and vary from subglacial and grounding line facies to more distal facies with ice rafting (Fairchild et al., 1989; Hambrey, 1982; Hoffman et al., 2012).

The Petrovbreen Member lacks direct geochronological constraints but has been correlated to the first glacial episode of the Cryogenian (Halverson et al., 2018; Hoffman et al., 2012), termed the Sturtian glaciation, based on a few lines of evidence. Chemical evidence to support the Sturtian age assignment comes from the similarity of the upper Russøya Member $^{87}Sr/^{86}Sr$ values to Tonian values (Hoffman et al., 2012) and corresponding stratigraphic association with a negative carbon isotope excursion identified as the Islay anomaly (Halverson et al., 2018; Hoffman et al., 2012). If the Sturtian correlation is valid, the upper Russøya Member was deposited between ~740 and 735 Ma (Halverson et al., 2018; MacLennan et al., 2018; but see Fairchild et al., 2017, for discussion of ambiguity in pre-Sturtian carbon isotope stratigraphy). Biostratigraphy further supports a pre-Sturtian correlation for the Russøya Member. Vase-shaped microfossils (VSM) are present in the Russøya Member in NE Svalbard (Knoll & Calder, 1983), similar to other pre-Sturtian strata where geochronology is well constrained (Cohen & Riedman, 2018; Strauss et al., 2014). Together, chemostratigraphy and biostratigraphy highlight the potential for these carbonates to record meaningful information about the onset of glacial conditions in the Cryogenian.

The burial history of Ny Friesland is poorly constrained, and the region was affected by the Caledonian Orogeny (Gasser, 2014, and references therein). Both Neoproterozoic and overlying Cambro-Ordovician strata are steeply dipping and faulted (Fairchild & Hambrey, 1984; Hoffman et al., 2012), but local organic preservation provides evidence for limited thermal alteration in the Cambro-Ordovician Oslobreen Group. Conodont color alteration indices are 1 (Bergström, 1980; Lehnert et al., 2013), where the Oslobreen Group disconformably overlies Neoproterozoic strata in NE Ny Friesland. Though empirical, such alteration indices are thought to indicate lower burial temperatures (Epstein et al., 1977). Limited thermal alteration is also evident from intact biomarkers of the Oslobreen Group strata, consistent with midoil window thermal maturity (RockEval Pyrolysis T_{max} values of 441–446°C; Lee et al., 2019). Midoil window constraints on burial temperatures (<150°C; e.g., Peters et al., 2005) would require burial depths less than or comparable to the 4–6 km of modeled exhumation of regional Caledonian granites since 80–180 Ma (Dörr et al., 2012; Dörr et al., 2019) from apatite fission track analysis. Heterogeneity in timing and rates of exhumation indicates that there is strong local fault control on tectonic histories across Ny Friesland (Dörr et al., 2012; Dörr et al., 2019). Local control on burial and exhumation histories indicates that preservation of temperature-sensitive records like biomarkers or carbonate clumped isotopes may be locally

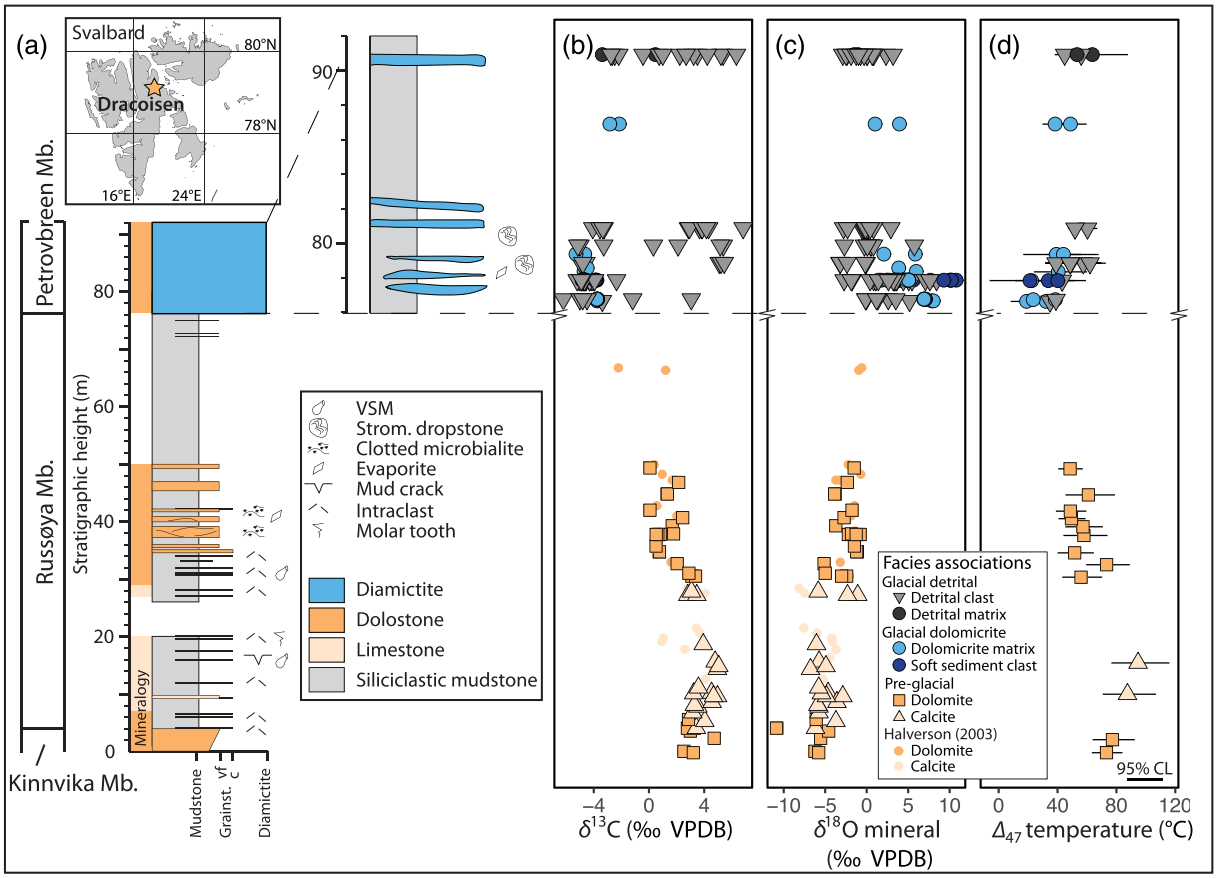

Figure 1. Stratigraphy of the latest Tonian (Kinnvika Member of the Backlundtoppen Formation and Russøya Member of the Elbobreen Formation) and earliest Cryogenian (Petrovbreen Member of the Elbobreen Formation) at the Dracoisen Nunatak, NE Svalbard. (a) Stratigraphic column highlighting transitions among the dominant carbonate mineralogies. The scale of the Petrovbreen Member is extended to display diamictite distribution. (b) Composite of δ^{13}C values and (c) mineral δ^{18}O value through stratigraphic section. (d) Clumped isotope temperatures and 95% CL error for a subset of these samples.

heterogeneous in pre-Caledonian strata but that more recent exhumation was not preceded by much deeper burial for at least some fault blocks. In order to avoid potential regional variability in clumped isotope preservation, we have restricted this study to one section spanning the Tonian-Cryogenian boundary on the Ny Friesland Dracoisen nunatak where Petrovbreen Member carbonates have the best textural preservation (Fairchild, 1983; Fairchild et al., 1989; Halverson et al., 2004, 2018).

2. Materials and Methods

2.1. Field Localities and Sampling

Carbonates from the Kinnvika Member of the Backlundtoppen Formation, Akademikerbreen Group, and overlying Russøya and Petrovbreen members of the Elbobreen Formation, Polarisbreen Group, were collected in stratigraphic context on the Dracoisen nunatak, NE Ny Friesland, Svalbard, on a field campaign in 2014 (GPS 79.204931, 18.345240) at a section previously studied, measured, and mapped by Fairchild et al. (1989) and Halverson et al. (2004). A stratigraphic section was measured, and, where present in the stratigraphy, carbonate samples were collected at approximately 1 m intervals where present (Table S1 in the supporting information). The collected sample suite was supplemented with four Petrovbreen Member samples from the Dracoisen nunatak previously collected by Ian Fairchild (University of Birmingham). Due to lateral lithofacies heterogeneity in Petrovbreen Member stratigraphy, these four samples were integrated into the stratigraphic section detailed in this study (Figure 1) based upon their stratigraphic height relative to marker beds.

2.2. Petrography and Mineral Identification

Carbonate samples were cut to remove weathered surfaces prior to petrographic and geochemical analysis. All samples used for clumped isotope analysis ($n = 24$) were slabbed, polished and scanned (Figure S1) to aid in the identification of target carbonate textures to drill for subsequent subsampling and analysis ($n = 41$). Of the 24 slabbed samples, 20 were thin sectioned for petrographic characterization of target textures. We further analyzed drill sites from 17 of 20 thin sections for mean crystal size using 25 representative crystals from each sampled carbonate texture. Measurements were made using ImageJ software from thin section photomicrographs following the method of Bergmann, al Balushi, et al., 2018 (Table S1). We describe carbonate microfacies after Fairchild et al. (1989) and adopt the terms [dolo]micrite in reference to carbonate crystals less than 10 μm in diameter, [dolo]microspar for crystals between 10 and 50 μm in diameter, and spar for mean crystal diameter >50 μm (cf. Flügel, 2004).

Sample mineralogy was determined based on X-ray diffraction (XRD) or dilute acid reaction (Table S1). For XRD, splits of powdered samples were analyzed on a PANalytical X'Pert PRO X-ray powder diffractometer (XRPD) housed in the Massachusetts Institute of Technology Center for Materials Science and Engineering (MIT-CMSE) to quantify the abundance of calcite, dolomite, and other minerals. For each sample, approximately 500 μg of powder was analyzed for 2 hr from 5° to 90° on a spinning stage at a fixed irradiated length.

2.3. Isotopic Analysis

Carbonate $\delta^{13}C$, $\delta^{18}O$, and clumped isotopic (Δ_{47}) analyses were performed at MIT on a Nu Perspective isotope ratio mass spectrometer coupled to a Nu Carb automated carbonate sampler. Samples of specific carbonate textures were drilled using carbide bits to produce homogeneous powders for isotopic analyses. Clumped isotope analysis had different methods from samples solely analyzed for bulk $\delta^{13}C$ and $\delta^{18}O$; these methods are presented separately below.

2.3.1. Carbonate Clumped Isotope (Δ_{47}) Analysis

For Δ_{47} measurements, we analyzed ~450 μg per sample replicate of carbonate powder drilled from polished sample slabs; weights for samples with lower weight percent carbonate as determined by CO_2 yield were increased to match the carbonate mass of the pure standards and ranged from ~450 to 900 μg. Carbonates were digested in sample vials with 150 μL H_3PO_4 (1.94–1.95 g/cm^3); see supporting information for detailed description of clumped isotope analytical methods (Text S1). Clumped isotope data were processed using Easotope software (John & Bowen, 2016), and ^{17}O corrections were made after Schauer et al. (2016) and Daëron et al. (2016). Raw $\delta^{13}C$, $\delta^{18}O$, and clumped isotopic (Δ_{47}) measurements were transferred to Vienna Peedee belemnite (VPDB) and Carbon Dioxide Equilibrium Scale (CDES) (Dennis et al., 2011), respectively, using carbonate standards ETH-1, ETH-2, ETH-3, and ETH-4 with an 11 standard moving window. The $\delta^{13}C$, $\delta^{18}O$, and Δ_{47} values of the ETH standards were cross referenced to international standards IAEA-C1, IAEA-C2, NBS-18, and NBS-19 and heated and equilibrated gases (Bernasconi et al., 2018). Calcite and dolomite Δ_{47} values were further corrected with a 70°C acid fractionation factor of 0.062 (Defliese et al., 2015; Müller et al., 2017). All samples passed screening for contamination using Δ_{48} values; all samples had Δ_{48} values with a lower absolute value than the cutoff of <0.5‰. Samples were only incorporated into this study where ≥3 replicates passed all screening tests (Text S2).

Analyses were carried out over the course of 1.5 years (June 2017 to November 2018), during which time instrument upgrades and repairs led to changes in precision of analyses. In the course of this study, long-term standard deviation of reference materials (1 SD) varied from 0.02‰ to 0.04‰, 0.02‰ to 0.07‰, and 0.06‰ to 0.20‰ for Δ_{47}, $\delta^{13}C$, and $\delta^{18}O$ values, respectively. Raw data for all standards and sample replicates are available in supporting information and are posted at EarthChem (DOI: 10.26022/IEDA/111534).

We calculated precipitation temperature following the Δ_{47}-temperature relationship of Bernasconi et al. (2018). Additional discussion of dolomite temperature calibrations is presented in the supporting information (Text S3). Precipitating fluid $\delta^{18}O$ values were calculated from mineral $\delta^{18}O$ values and Δ_{47} temperatures, assuming equilibrium fractionation between fluid and mineral $\delta^{18}O$ following the temperature-fractionation relationship of S.-T. Kim and O'Neil (1997) for calcite and Horita (2014) for dolomite. Reconstructed fluid $\delta^{18}O$ values are reported relative to Vienna Standard Mean Ocean Water (VSMOW). Error for clumped isotope temperatures are presented as 95% confidence levels from sample

replicates (Fernandez et al., 2017) for conservative estimates of error in reconstruction, whereas the mean of populations of genetically related samples are listed with errors of one standard deviation.

2.3.2. Carbonate $\delta^{13}C$ and $\delta^{18}O$ Microvolume Analysis

Samples of ~100 μg carbonate were analyzed for $\delta^{13}C$ and $\delta^{18}O$. Samples spanned the Dracoisen stratigraphy at the m-scale resolution of sampling, and select carbonate textures analyzed for Δ_{47} were drilled at the mm scale to assess compositional heterogeneity (Figure S2. Microvolume analysis of drilled samples consisted of digestion in H_3PO_4 (1.91–1.92 g/cm^3) at 70°C, followed by cryogenic purification. Sample beam analysis consisted of six cycles of 20 s integration. Results were processed using Easotope software (John & Bowen, 2016) translated to the VPDB reference frame using ETH standard materials. ETH standards were cross referenced to international standards IAEA-C1, IAEA-C2, NBS-18, and NBS-19 (Bernasconi et al., 2018). Long-term standard deviation of reference materials (1 SD) throughout the course of analysis (January 2018 to September 2018) varied from 0.04–0.09‰ and 0.07–0.17‰ for $\delta^{13}C$ and $\delta^{18}O$, respectively, in individual correction intervals.

3. Results

3.1. Carbonate Petrography

The stratigraphic distribution of facies documented in our study of the Dracoisen nunatak complements and expands upon those of previous authors (Fairchild et al., 1989; Halverson et al., 2004, 2018); we utilize both facies associations and our petrographic observations to assign carbonates, and the associated isotope analyses, to preglacial and synglacial paleoenvironmental classes (Figure 2).

Preglacial carbonates comprise the lowest stratigraphic section examined in this study. The upper Kinnvika Member is here composed of stylotized dolomicrospar (mean crystal sizes 14–23 μm), with local sheet crack-filling dolospar. The Kinnvika Member transitions upward to limestones of the lower Russøya Member, which are composed of microspar and intraclastic grainstone. Rare mud cracks and molar tooth textures are also present. Up section, Russøya Member carbonates change to dolostone composed of stromatolites with a clotted microtexture, intraclastic grainstone and evaporite pseudomorphs. The crystal size of Russøya Member dolomites varies with texture. The finest dolomicrites (<5 μm) are present in stromatolite clots, whereas laminated dolomites are typically micritic to microsparitic (mean crystal sizes 17 ± 8 μm, 1 SD), including laminae intercalated on the mm scale with the finest dolomitic clots.

The overlying Petrovbreen Member carbonates analyzed here are dolomitic, with varying contribution of chert clasts, siliciclastic mudstone, and subsidiary siliciclastic grains. Siliciclastic grains include rare grain aggregates, which we have interpreted as till pellets (Figure S3), consistent with the prevailing interpretation of a glaciomarine or glaciolacustrine depositional environment (Fairchild et al., 1989; Halverson et al., 2018; Hambrey, 1982). Dolomites consist of three components defined by their crystal/grain size, texture, and relationship to surrounding sediments: (1) dolomicrite, (2) large angular to well-rounded clasts, and (3) small clasts making up the matrix around large clasts.

1. Dolomicrite (mean crystal size <5 μm) is present in the Petrovbreen Member as homogeneous beds, interlaminated with coarser carbonate grains in thinly laminated couplets, within ductily deformed soft sediment clasts, or as a matrix between larger clasts. Dolomicrite matrix is present in both stratified diamictites and matrix-supported diamictite samples without lamination or clast sorting. Dolomicrite purity varies in samples analyzed by XRD, with compositions ranging from >70% dolomite to a subsidiary component mixed with more abundant quartz as well as other silicate minerals (Table S2). Dolomicrite is most abundant in the lowermost 2 m of the Petrovbreen Member below a brecciated surface (I. J. Fairchild, personal communication, March 2017) containing abundant pseudomorphs consistent with sulfate minerals. Additional dolomicrite is present above this surface as homogeneous dolomicrite, diamictite matrix, and fine rhythmite laminae.
2. Greater than 1 mm angular to well-rounded clasts with constituent carbonate fabrics that are stromatolitic, clotted, fenestral, laminated, intraclastic, and dolomicritic. These larger angular to well-rounded clasts are hereafter referred to as detrital clasts. Detrital clasts have a range of mean crystal sizes, with stromatolitic, clotted, fenestral, laminated, and intraclastic carbonate fabrics having mean crystal sizes ≥10 μm in contrast to the finer dolomicrites. Rare detrital clasts from the stratified diamictite have circumgranular sparry crusts up to 100 μm thick (Figure S3).

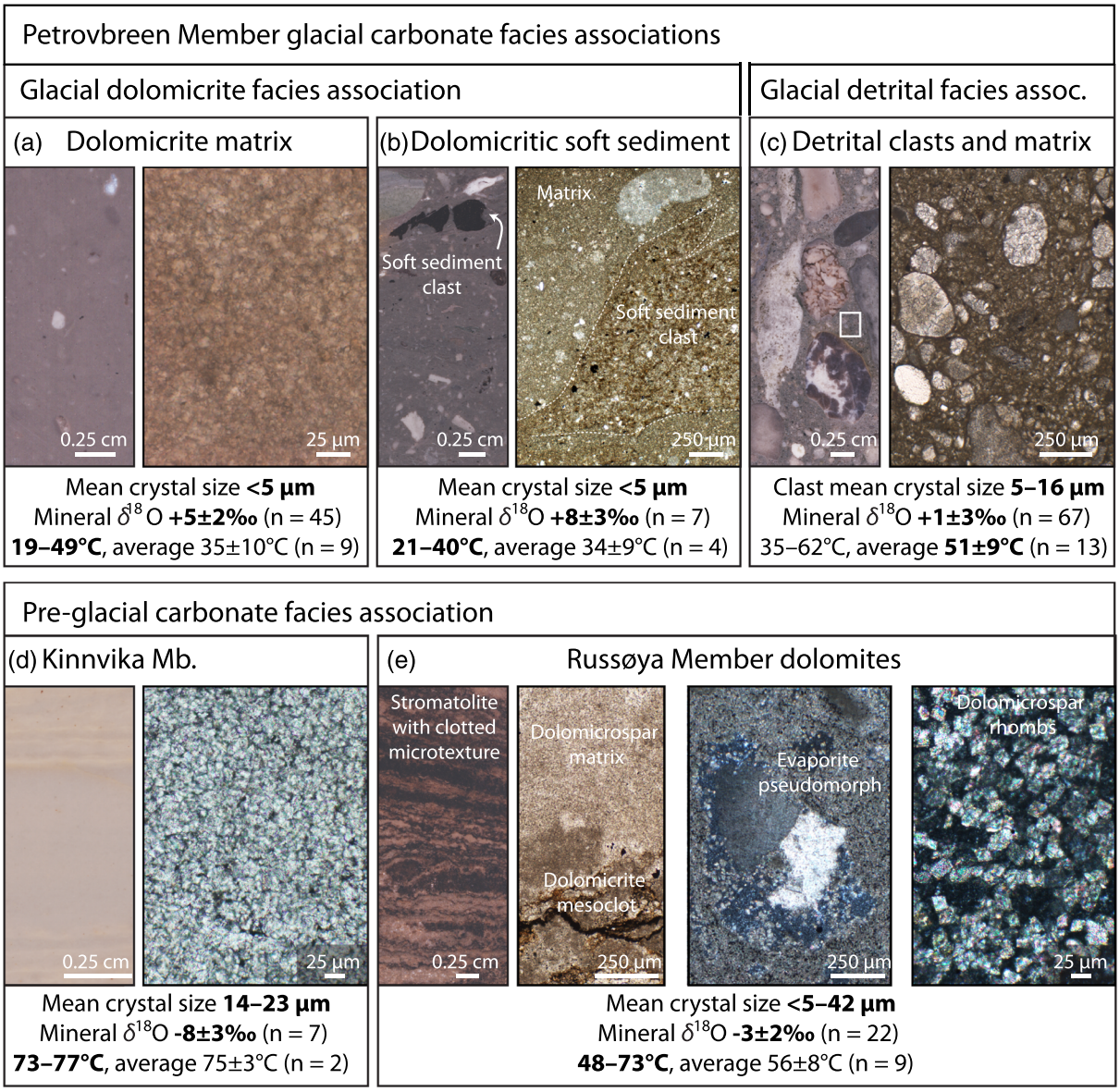

Figure 2. Petrographic textures of the Dracoisen section dolomites; where images are paired, left is a scanned polished sample and right is thin section photomicrograph. (a–c) Glacial carbonates of the Petrovbreen Member consisting of (a) homogeneous dolomicrite matrix, (b) discrete dolomicritic soft sediment clasts in diamictite, and (c) detrital clasts and matrix consisting of <1 mm detrital grains. (d and e) Preglacial carbonates of the (d) peritidal Kinnvika Member of the Akademikerbreen Formation and (e) overlying Elbobreen Formation Russøya Member. Russøya Member dolomite facies pictured here include stromatolites with a clotted microtexture, evaporite pseudomorphs partially replaced by dolomite and silica (here cross polarized to highlight twinning after gypsum) and homogeneous dolomicrospar rhombs in wedged thin section. Mean crystal sizes indicate range in mean sizes for analyzed samples, and isotope data present the mean mineral $\delta^{18}O$ values and clumped isotope temperatures ±1 standard deviation to describe the population analyzed and the range of mean clumped isotope temperatures.

3. Carbonate grains <1 mm, which form the matrix between the larger detrital clasts. Dolomite components vary stratigraphically. The majority of Petrovbreen Member carbonates consist of detrital clasts from Groups 2 and 3 in diamictite beds or dropstones in siliciclastic mudstone (Figure 1a).

Together, the Dracoisen stratigraphy comprises three broad facies associations. The Kinnvika and Russøya members make up: (1) preglacial facies association, which are possible source strata for subsequent glacial erosion and redeposition. The Petrovbreen Member carbonates make up two facies associations based on petrographic texture: (2) the glacial dolomicrite facies association includes homogeneous dolomicrite, dolomicrite matrix, soft sediment clasts, and thinly laminated couplets; (3) the glacial detrital facies association

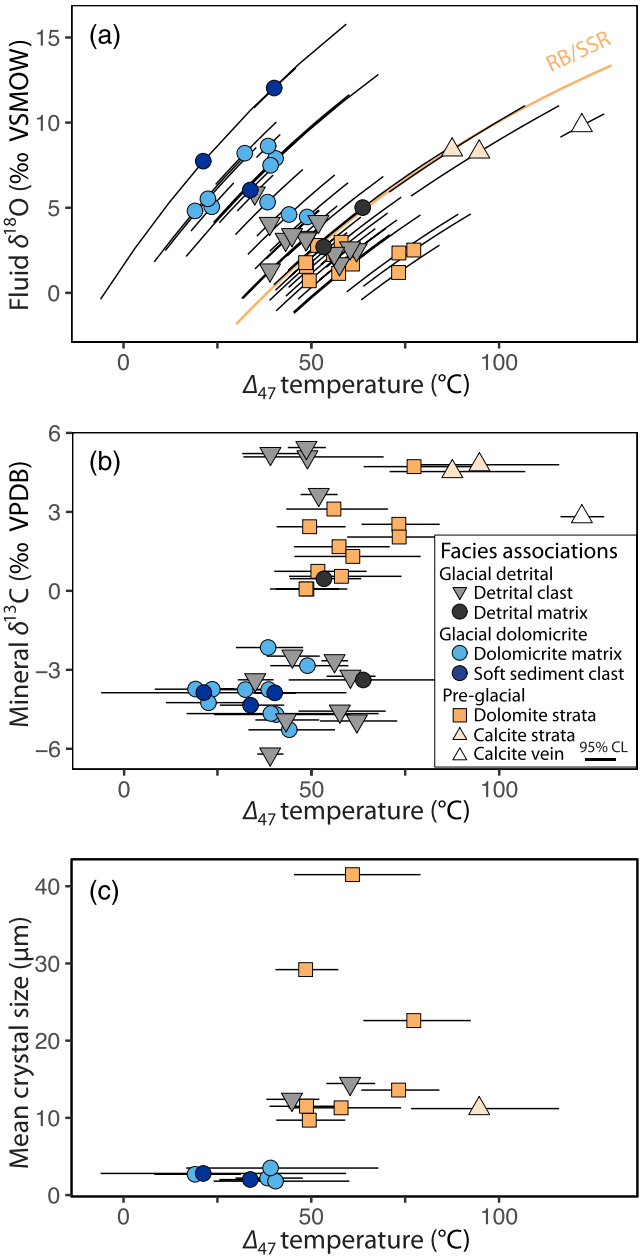

Figure 3. Summary of standard and clumped isotope values with petrographic observation. (a) Measured clumped-isotope temperature for carbonate samples versus the reconstructed fluid $\delta^{18}O$ values. Ninety-five percent CL error bars are diagonal due dependence of reconstructed fluid $\delta^{18}O$ values on measurement temperature. RB/SSR line denotes reconstructed fluid composition for dolomites (Horita, 2014) under purely rock-buffered alteration or solid-state reordering, given a starting fluid composition of −1.2‰. (b) Measured clumped isotope temperature versus mineral $\delta^{13}C$. (c) Mean crystal size varies with clumped isotope temperatures. Mean crystal size of diamictite clasts is consistent with the source stratigraphy inferred from reconstructed $\delta^{18}O$ fluid values and clumped-isotope temperatures. Calcite versus dolomite mineralogy does not appear to correspond to a significant difference in mean crystal size, despite elevated calcite temperatures interpreted as evidence of solid-state reordering. Crystal sizes <5 µm are approximate due to thickness of petrographic thin sections.

includes both the larger detrital dolomite clasts and matrix material composed of recognizable finer <1 mm dolomite clasts. The geochemistry of these three facies associations are detailed in the following sections.

3.2. Isotope Analyses of Preglacial Sediments

Carbonate $\delta^{13}C$ and $\delta^{18}O$ isotopic composition vary stratigraphically (Figures 1b and 1c), and results presented here are in agreement with previously published studies of these strata (Figures 1 and 4; Halverson, 2003; Halverson et al., 2005, 2007). $\delta^{13}C_{VPDB}$ values greater than +2‰ characterize the Kinnvika and lowermost Russøya members. $\delta^{13}C$ values peak at +5.1‰ in the calcite strata of the lower Russøya Member and decrease to +0.5‰ over 20 m of section through the transition to dolomite. $\delta^{13}C$ values in the subsequent dolomite beds remain between +0.1‰ and +2.4‰ through the transition to shale in the upper Russøya Member. Mean mineral $\delta^{18}O_{VPDB}$ values increase through the Kinnvika and Russøya members, from −7 ± 2‰ (1 SD) in the Kinnvika Member, to −5 ± 2‰ (1 SD) in the lower Russøya Member calcites and −2 ± 1‰ (1 SD) in the overlying Russøya Member dolomites (Figures 1 and 3 and Table S1).

Reconstructed clumped isotope temperatures through the preglacial facies also show distinct trends across lithology and depositional environment (Figure 1d). Where calcite beds and veins cooccur in the Russøya Member, these samples record warmer temperatures than Russøya Member dolomites.

Calcite samples from bedded strata and crosscutting veins record mean temperatures of 92 ± 5°C ($n = 2$, 1 SD) and 122 ± 6°C (95% CL), respectively (Figure 3a). Dolomites in preglacial strata preserve a range of clumped isotope temperatures from 48°C to 77°C (Figure 1d and Table S1). Peritidal facies of the Kinnvika member record higher temperatures (75 ± 3°C, $n = 2$, 1 SD) compared to the immediately overlying Russøya Member dolomites (56 ± 8°C, $n = 9$, 1 SD) (Figure 1d and Table S1).

Reconstructed fluid compositions calculated from mineral $\delta^{18}O$ and clumped isotope temperatures also vary by facies and mineralogy across the preglacial stratigraphy (Figure 3a). Samples of the Kinnvika member have reconstructed fluid $\delta^{18}O_{VSMOW}$ compositions of +1.9 ± 0.9‰ (1 SD, $n = 2$, Table S1). Reconstructed fluid composition of the Russøya Member varies with mineralogy (Figure 3a): calcite reconstructed fluid $\delta^{18}O_{VSMOW}$ values are +8.3 ± 0.1‰ (1 SD, $n = 2$), whereas Russøya Member dolomites have reconstructed fluid $\delta^{18}O_{VSMOW}$ values from +0.7‰ to +3.0‰ (+1.9 ± 0.8‰, 1 SD $n = 9$, Table S1).

3.3. Isotope Analyses of Glacial Dolomicrites

Relative to the underlying preglacial stratigraphy, dolomicrite of the Petrovbreen Member has negative $\delta^{13}C_{VPDB}$ (−4.4 ± 0.6‰, 1 SD $n = 45$) and positive $\delta^{18}O_{VPDB}$ values (+5 ± 2‰ 1 SD $n = 45$), consistent with observations of Fairchild et al. (1989). The fine-scale isotopic variability of this dolomicrite differs between matrix-supported and stratified diamictite samples. The dolomicrite of matrix supported diamictite is isotopically homogeneous where subsampled

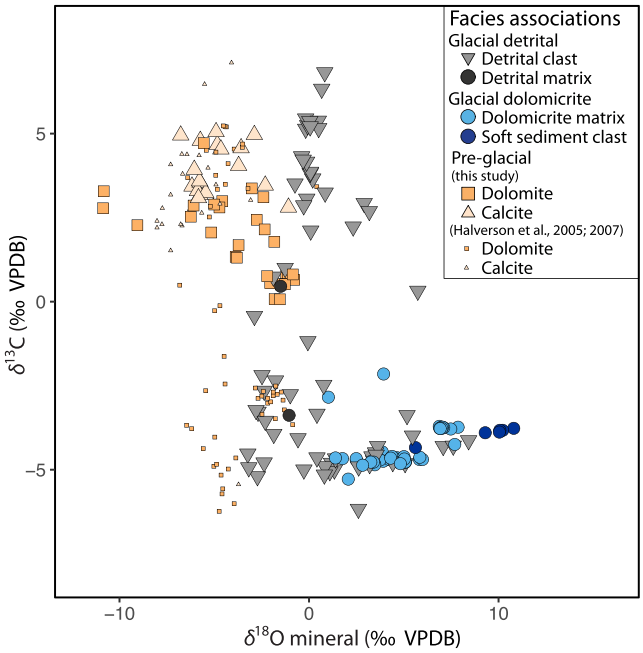

Figure 4. Cross plot of carbonate δ^{13}C and δ^{18}O values from the Tonian-Cryogenian in NE Svalbard. Preglacial carbonates from Halverson et al. (2005, 2007) sample the Russøya Member. Regionally, the Russøya Member displays a broader δ^{13}C and δ^{18}O range than the Dracosien nunatak section. δ^{13}C and δ^{18}O values for the underlying Akademikerbreen Formation are presented in Figure S4. Glacial Petrovbreen Member carbonates sampled here are exclusively dolomitic. Diamictite clasts span the full range of δ^{13}C values in the underlying stratigraphy but are generally more enriched in ^{18}O. Heterogeneous Petrovbreen Member carbonate isotopic values are consistent with multiple carbonate sources, here interpreted as a detrital carbonate source with comparable δ^{18}O values to underlying nonglacial stratigraphy and a glacial source with higher δ^{18}O values.

for microvolume analyses, with $\delta^{13}C_{VPDB}$ and $\delta^{18}O_{VPDB}$ values within analytical uncertainty (−3.75 ± 0.02‰ and +6.98 ± 0.08‰, respectively, 1 SD $n = 8$). Where dolomicrite forms the matrix of stratified diamictites 1 m above the matrix supported diamictite, $\delta^{18}O_{VPDB}$ values vary at the mm scale through stratified layers, from +1.4‰ to +7.7‰ (mean +4.1 ± 1.2‰, 1 SD $n = 29$). $\delta^{13}C_{VPDB}$ values are more consistent, with a mean of −4.7 ± 0.1‰ (1 SD $n = 29$). Within the same sample, soft sediment clasts have similar $\delta^{13}C_{VPDB}$ values as the mean matrix dolomicrite (−3.9 ± 0.2‰ 1 SD $n = 6$) but with higher $\delta^{18}O_{VPDB}$ values (+9.4 ± 1.8‰ 1 SD $n = 6$; Figure S2).

Matrix dolomicrite clumped isotope temperatures range from 19°C to 49°C, with mean temperatures 35 ± 10°C ($n = 10$, 1 SD; Figures 1d and 3a). Within a hand sample, dolomicrite with coarser crystal sizes associated with local alteration (Fairchild, 1983) has warmer clumped isotope temperatures than in adjacent finer dolomicrite (49 + 11/−10°C vs. 38 ± 9°C, 95% CL; Table S1). Clasts featuring soft sediment deformation also have clumped isotope temperatures similar to the dolomicrite matrix, ranging from 21°C to 40°C (31 ± 10°C, $n = 3$, 1 SD, Figure 1d and Table S1). The reconstructed fluid $\delta^{18}O_{VSMOW}$ values for the lowest temperature (<25°C, $n = 4$) dolomicrite samples and soft sediment clasts range from +4.8‰ to +7.7‰ (Figure 3a).

3.4. Glacial Detrital Facies Association Isotope Analyses

Clumped isotope temperatures and δ^{13}C and δ^{18}O values of detrital clasts span much of the range of both the preglacial and glacial dolomicrite facies associations (Δ_{47} 35–62°C, $n = 12$; $\delta^{13}C_{VPDB}$ −5.2‰ to +6.8‰, and $\delta^{18}O_{VPDB}$ −3.2‰ to +8.4‰, $n = 68$; Figures 1, 3, and 4). Comparable clumped isotope temperatures and δ^{18}O values between detrital clasts and surrounding stratigraphy correspond to a similar range of reconstructed fluid $\delta^{18}O_{VSMOW}$ values (+1.3‰ to +5.9‰; Figure 3a). Where the diamictite matrix is composed of fine detrital clasts, the δ^{13}C and δ^{18}O values are comparable to the surrounding detrital clasts (Figure 4). These samples also have clumped isotope temperatures similar to the warmest clasts (59 ± 7°C, $n = 2$, 1 SD; Figures 3a and 3b).

Clumped isotope temperatures and mineral δ^{18}O values also correlate with carbonate texture. As previously documented by Fairchild et al. (1989), detrital clasts that resemble preglacial strata with stromatolitic, clotted, or fenestral textures share similar isotopic compositions with them: $\delta^{18}O_{VPDB}$ values span −3.2‰ to +0.8‰ for seven such clasts, and their clumped isotope temperatures range from 39°C to 62°C (Table S1).

4. Discussion

Our samples of Tonian and Cryogenian carbonates from the Dracoisen nunatak preserve information about the timing and style of their diagenesis through petrographic textures and isotopic compositions, consistent with previous work in these strata (e.g., Fairchild et al., 1989). In the following discussion, we explore (1) the utility of clumped isotope record to identify diagenetic processes that have affected these carbonates and (2) the potential for carbonate isotopic compositions to inform on Earth system changes through the Cryogenian.

4.1. Evidence for Solid-State Reordering

Carbonate clumped isotope composition varies systematically across carbonate facies, petrographic relationships, and mineralogies. Within the preglacial Russøya Member, clumped isotope temperatures and reconstructed fluid compositions are higher in calcite than dolomite (Figure 3). This mineral-dependent relationship is consistent with the preferential solid-state reordering of calcite at lower temperatures than

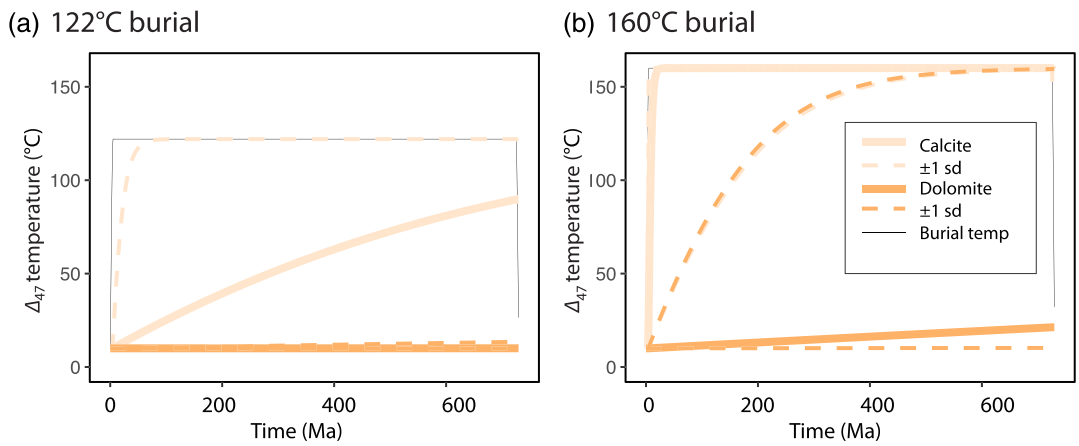

Figure 5. Modeled clumped isotope temperature change for calcite and dolomite with hypothetical burial for 730 Ma to 122°C (a) and 160°C (b) with the Passey and Henkes (2012) solid-state reordering linear approximation model in ClumpyCool for Python (after Lloyd et al., 2018). Calcite kinetic parameters follow Passey and Henkes (2012), and dolomite parameters follow Lloyd et al. (2018). Following modeled parameters, calcite partially (a) or fully (b) reorders to burial conditions whereas dolomite alteration is limited.

dolomite (Lloyd et al., 2018; Passey & Henkes, 2012; Stolper & Eiler, 2015). Calcite vein cement (122 ± 6°C; 95% CL) provides a minimum burial temperature estimate, and the maintenance of lower temperatures (92 ± 5°C; $n = 2$, 1 SD) in adjacent calcite strata indicates that peak burial temperatures did not reach temperatures necessary to fully reorder calcite. Based on laboratory reordering experiments and field observations, over 100 Ma calcite begins to be impacted at ~100°C, and calcites are 99% reordered at 144°C (values for brachipod calcite, Passey & Henkes, 2012; Henkes et al., 2014).

We explored the effect of solid-state reordering over the longer potential burial history of Svalbard strata with Passey and Henkes' (2012) linear approximation model for reordering using the ClumpyCool time-temperature model for Python (Lloyd et al., 2018; https://github.com/maxmansaxman/Clumpy_reordering_model_distribution). Arrhenius parameters for calcite come from Passey and Henkes (2012). For a simple 730 Ma burial history to 122°C with 5 Ma burial and exhumation, initial 10°C calcite clumped isotope temperatures gradually increase to 90°C (Figure 5). With a comparable burial history to higher temperatures of 160°C, calcite temperatures exceed observations (92 ± 5°C) within 8 Ma and approach equilibrium with burial temperatures of 160°C by 20 Ma (Figure 5). Although these models have unrealistic uniform burial conditions, they do constrain the rates at which carbonates would equilibrate to burial conditions. Differences in calcite temperatures between veins and adjacent strata indicate that Dracoisen carbonates are unlikely to have exceeded temperatures of 160°C for a significant part of their burial history. The kinetics of reordering would lead to rapid equilibration of calcite to higher temperatures than observed, even with relatively short excursions (<10 Ma) to burial temperatures of 160°C.

Burial temperatures reflected by partial calcite reordering are within the upper bounds predicted for preservation of dolomite clumped isotope temperatures based on experimental reordering kinetics (Lloyd et al., 2018). Within the 122°C 730 Ma burial model described above, dolomite clumped isotope temperatures remain unchanged; burial at 160°C leads to minor increase in temperature from the initial 10°C to 21°C (Figure 5). In contrast to limited dolomite alteration in these models, observed preglacial dolomite temperatures exceed expectations for reasonable surface conditions (48–77°C). Such high temperatures could result from (1) timing of dolomite precipitation under deeper burial conditions, (2) diagenetic alteration with partial dissolution and reprecipitation with burial, or (3) uncertainties in reordering kinetics over the long burial histories relevant to Neoproterozoic strata. Regarding this last point, uncertainties in existing models are large, and the 1 SD envelope for the models listed above exceed the variability in clumped isotope data observed in this study (Figure 5). More complex models that account for initial annealing of defects (Henkes et al., 2014) behave similarly to the linear approximation model of Passey and Henkes (2012) at burial temperatures below 150°C. However, the two-step reaction diffusion model of Stolper and Eiler (2015) for calcites predicts limited reordering at lower burial temperatures (0–25°C) prior to higher temperature

alteration. This model also predicts lower-temperature dolomite reordering, which may be more consistent with our observed dolomite temperature ranges. Additional work is necessary to refine models comparing calcite and dolomite solid-state reordering over deep time, particularly with field studies where clumped isotopes can be compared to other proxies of thermal maturation (Bergmann, al Balushi, et al., 2018; Lacroix & Niemi, 2019; Naylor et al., 2019). In the following discussion, we assess the relationships among petrographic textures, bulk isotope compositions, and clumped isotope temperatures in both glacial and preglacial facies to further constrain diagenetic contributions to the clumped isotope record.

4.2. Timing of Dolomite Precipitation

Preglacial and glacial carbonates have distinct petrographic textures, δ^{18}O, and δ^{13}C values. Carbonates from the preglacial and glacial dolomicrite facies associations cluster separately by these metrics, but the detrital glacial facies association contains clasts that display similar petrographic texture, crystal size distribution, and isotopic composition with both glacial dolomicrites and preglacial dolomites (Figures 3 and 4, consistent with Fairchild et al., 1989). The wide range of δ^{13}C values found in Russøya Member carbonates regionally < -4.5 to $> +7$‰; Hoffman et al., 2012; Halverson et al., 2018) is consistent with the composition of carbonate clasts found in the Petrovbreen Member. Indeed, clasts with distinctive petrographic textures, such as stromatolite morphologies like those found regionally in the nadir of the pre-Sturtian "Islay" negative carbon isotope excursion (Hoffman et al., 2012; Table S1), have low δ^{13}C values (< -4.5‰) and low mineral δ^{18}O values consistent with the underlying interpreted source stratigraphy. Some stratified diamictite samples also contain clasts compositionally and texturally similar to the glacial matrix dolomicrite (Figure S2). These relationships are consistent with clasts sourced from both underlying strata and local reworking of dolomicrite material in the depositional environment.

The high δ^{18}O values of the Petrovbreen Member dolomicrite are distinct from other dolomites in this stratigraphic section. The fine size of dolomicrite crystals has previously been interpreted as evidence for deposition as detrital carbonate rock flour (Fairchild, 1983); however, the coincidence of high δ^{18}O and low δ^{13}C mineral values in the diamictite matrix differs from the regional composition of dolomitic strata that could serve as the rock flour protolith (Halverson et al., 2018; Figure S4). Instead, we interpret the Petrovbreen Member dolomicrite as an end-member carbonate facies that reflects formation during glacial conditions. This interpretation is also consistent with the petrographic evidence for extremely fine crystal sizes and soft sediment deformation and is more consistent with the unique isotopic compositions. The isotopic composition of fine-grained glacial strata clasts then would fall on a mixing line between the preglacial strata and this glacial dolomicrite facies (Figures 4 and S2). The glacial dolomicrite end-member isotopic composition is also geochemically distinct from the overlying postglacial Petrovbreen cap dolostone and dolomitic silt shale of the MacDonaldryggen Member, which have lower δ^{18}O values than the glacial dolomicrite (-8.6‰ to $+0.6$‰ with a mean of -3.7‰; Fairchild, Bonnand, et al., 2016; Figure S4). Petrography of postglacial dolomite indicates that MacDonaldryggen Member dolomite precipitation predated compaction; pore-filling calcite, interpreted as later burial cements, are also associated with more negative δ^{18}O values around -9‰ (Fairchild, Bonnand, et al., 2016).

Δ_{47} temperature heterogeneity is maintained on the scale of clasts versus matrix material in a clumped isotope conglomerate test (Figure S1), with temperatures of $\leq$25°C ($n = 4$) restricted to Petrovbreen Member samples of matrix dolomicrite and clasts featuring soft sediment deformation (mean Δ_{47} temperature of 34 ± 9°C, 1 SD $n = 14$; Figures 1d and 4) relative to a mean temperature of 50 ± 9°C (1 SD $n = 11$) in detrital clasts. Such heterogeneity indicates that dolomites represent distinct populations with different depositional or early diagenetic histories. Temperature differences between the clasts and matrix of Petrovbreen Member diamictite require that dolomitization of clasts predated redeposition in the diamictite; dolomitization would affect clumped isotope composition of carbonates, even under low water-rock conditions that could have preserved carbonate δ^{18}O values from early lithification (e.g., Ferry et al., 2011). The distinct petrographic characteristics and stable isotope composition of glacial dolomicrites indicate that they do not share a common diagenetic source with overlying and underlying dolomites, despite their close stratigraphic association (Figure 1).

Δ_{47} temperatures of Petrovbreen Member dolomicrite further constrain the source and timing of dolomite formation. Temperatures as low as $19 + 12/-11$°C (95% CL) are inconsistent with precipitation or

recrystallization in deep burial conditions during nonglacial periods (e.g., Kupecz et al., 1993), particularly given low reconstructed paleolatitudes (Maloof et al., 2006). Thus, the composition of the glacial dolomicrite facies association is consistent with a distinct carbonate precipitating at low temperatures from a fluid with a higher $^{18}O/^{16}O$ ratio than associated detrital dolomite clasts. Evidence for early dolomitization in both the Russøya and Petrovbreen members is consistent with studies of Tonian carbonates in Svalbard (Knoll & Swett, 1990) and other Neoproterozoic strata (Hood et al., 2011; Shuster et al., 2018; Tucker, 1982). The scattered yet enriched reconstructed fluid compositions of $\delta^{18}O_{VSMOW}$ values between +4‰ and 12‰ will be discussed in section 4.4.

4.3. Clumped Isotope Evidence for Style of Dolomite Diagenetic Alteration

Despite evidence for early dolomite precipitation (section 4.2) and limited alteration expected from solid-state reordering (section 4.1), preglacial dolomite clumped isotope temperatures vary from 48–77°C. The Kinnvika Member dolomites have higher mean Δ_{47} temperatures (75 ± 3°C, 1 SD $n = 2$) and more uniformly coarse dolomite textures than the Russøya Member dolomites (56 ± 8°C, 1 SD $n = 9$), suggesting that they may have experienced differences in their diagenesis. Despite these apparent differences and higher Kinnvika Member mineral $\delta^{18}O$ values, mean reconstructed fluid $\delta^{18}O_{VSMOW}$ values are similar in both the Kinnvika and Russøya members at 2 ± 1‰. This relationship of temperature variability with consistent fluid composition is consistent with fluid-buffered diagenetic alteration wherein carbonates equilibrate to fluid $\delta^{18}O$ under elevated burial temperatures (Bergmann, al Balushi, et al., 2018; Ryb & Eiler, 2018; Staudigel & Swart, 2019; Winkelstern & Lohmann, 2016).

The lowest Δ_{47} temperature samples of the Russøya Member (48–52°C, $n = 4$) are significantly above temperatures expected for early diagenetic environments, indicating either rock-buffered diagenesis or partial solid-state reordering. If diagenetic fluids have rock-buffered $\delta^{18}O$ values, then differentiation of rock-buffered diagenesis would be difficult to distinguish from possible partial solid-state reordering based on isotopic composition alone (section 4.1) due to comparable results of increased Δ_{47} temperature without an associated change in mineral $\delta^{18}O$ values (e.g., Cummins et al., 2014; Lacroix & Niemi, 2019; Staudigel & Swart, 2019; Winkelstern & Lohmann, 2016). Stratigraphically, however, partial solid-state reordering and rock-buffered diagenesis could leave different patterns of alteration. The extent of rock-buffered diagenesis varies significantly with carbonate permeability (Bergmann, al Balushi, et al., 2018; Budd, 1989), which is itself a product of carbonate facies and petrographic texture (e.g., Jennings et al., 2000; Moore, 1989). Solid-state reordering, however, is a product of the time-temperature path through burial and exhumation (e.g., Henkes et al., 2014; Lloyd et al., 2018; Stolper & Eiler, 2015), which varies regionally (e.g., Lacroix & Niemi, 2019; Naylor et al., 2019), rather than on the m-scale stratigraphically or with petrographic texture. Kinetics of solid-state reordering do not appear to differ significantly with carbonate composition, as demonstrated by similar heating experiment results among carbonates with different impurities such as brachiopod calcite versus optical calcite (Henkes et al., 2014; however, see Passey & Henkes, 2012, and Stolper & Eiler, 2015, for discussion of trace element effects). Thus, although it is possible that partial solid-state reordering has affected clumped isotope temperatures given uncertainties in burial history and dolomite solid-state reordering kinetics (e.g., Lloyd et al., 2018; Stolper & Eiler, 2015), the finer-scale stratigraphic differences in Δ_{47} temperature associated with clear textural changes are more consistent with rock-buffered alteration.

Rock-buffered alteration through burial could include dissolution and reprecipitation or occlusion of microporosity (e.g., Moshier, 1989; Staudigel & Swart, 2019), even with the interpreted early lithification and shallow diagenesis for these dolomites. Criteria for recognizing diagenetic alteration in micritic carbonates are more ambiguous than fossil material (e.g., Gilbert et al., 2017; Myers et al., 2018; Wenzel et al., 2000). Comparison of preglacial and glacial dolomite isotopic compositions provides insight to the extent of alteration experienced by glacial strata and their potential to preserve $\delta^{18}O$ values from their early lithification and diagenesis. Glacial dolomites formed in a significantly different depositional environment from preglacial facies and experienced a similar deep burial history, but reconstructed fluid $\delta^{18}O$ values vary more in the glacial dolomicrites than in the preglacial dolomites (Figure 3). Part of the >7‰ variation in glacial dolomicrite reconstructed fluid $\delta^{18}O$ values is likely a result of varying proportions of detrital versus autochthonous carbonate, given the difference between detrital clast composition and glacial dolomicrites (Figure 3). In this case, detrital influence is predicted to coincide with lower mineral $\delta^{18}O$ values, as is apparent in the

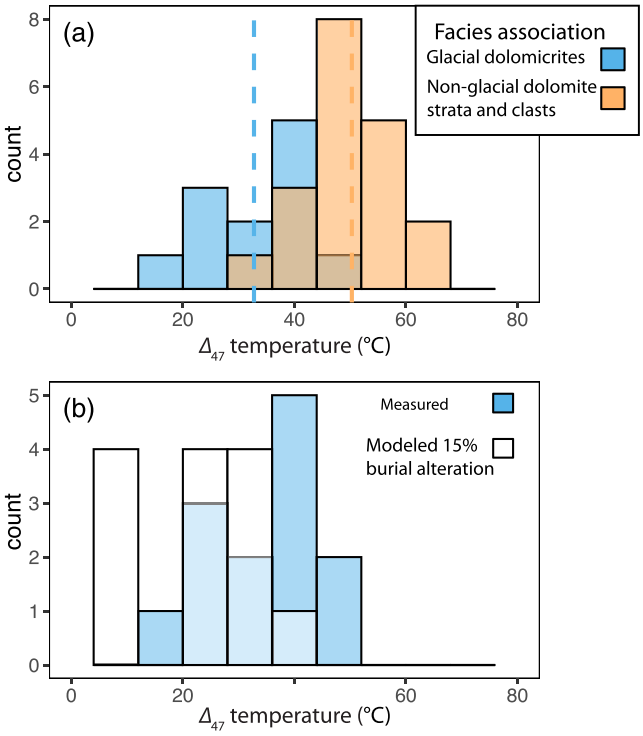

Figure 6. Histograms of clumped isotope data and reconstructions of initial conditions assuming partial rock-buffered alteration with burial. (a) Histograms of glacial dolomicrite and aggregated preglacial dolomite and diamictite clast facies; vertical lines mark mean Δ_{47} temperatures. (b) Glacial dolomicrite clumped isotope temperatures transformed with a modeled 15% contribution of dolomite equilibrated to burial temperatures, consistent with the interpreted alteration in preglacial carbonates (Table 1).

covariation of δ^{18}O values with depositional layering in stratified diamictites (Figure S2), and higher clumped isotope temperatures. Other glacial dolomicrite samples that have higher reconstructed fluid δ^{18}O values at higher temperatures (Figure 3) follow expected patterns for low water/rock ratio alteration buffered by the isotopic composition of the glacial dolomicrites.

Changes to the extent or style of dissolution and reprecipitation are not sufficient to explain the lower temperatures and more enriched δ^{18}O values of glacial dolomicrite facies compared to the underlying preglacial dolomites. Reconstructed fluid δ^{18}O values for glacial facies are higher than inferred for diagenetic fluids from the preglacial facies (Figure 3), and rock-buffered alteration with burial or dolomitization by basinal brines would lead to higher reconstructed fluid δ^{18}O values at greater temperatures (e.g., Mangenot et al., 2018). Instead, the Petrovbreen Member dolomicrite reconstructed fluid δ^{18}O values are higher at lower temperatures, consistent with precipitation from different early lithifying or diagenetic fluids prior to deep burial. In the following discussion of isotopic composition with facies, we only consider carbonates that display both petrographic and isotopic evidence for rock-buffered diagenesis. Excluded samples have isotopic evidence for high temperature fluid-buffered alteration (≥73°C, $n = 3$) and coarse dissolution and reprecipitation textures inconsistent with the textural preservation of surrounding strata ($n = 2$, one glacial, one preglacial; Table S1).

4.4. Coincidence of Facies Changes, δ^{18}O Composition, and Δ_{47} Temperature

As evident in the elevated temperatures from preglacial strata (section 4.3), dolomite clumped isotope temperatures have been impacted through burial. Despite this alteration, temperatures do covary with independent sedimentary records of climate; the coldest reconstructed clumped isotope temperatures of Russøya Member preglacial dolomite are 29°C warmer than the coldest temperatures recorded in the diamictite dolomicrite matrix. Comparing the Russøya and Petrovbreen Member temperatures, mean preglacial temperatures are significantly warmer than glacial dolomicrites. The mean temperature of the preglacial facies is between 16°C and 36°C warmer than glacial dolomicrite by the Welch Two Sample t test ($n = 19$, 95% confidence level), excluding the altered dolomites. This relationship is similar when all detrital clasts are binned with the preglacial facies, giving a mean temperature between 12°C and 29°C warmer than glacial dolomicrite ($n = 31$, 95% confidence level; Figure 6a).

The traditional carbonate δ^{18}O thermometer for dolomites (fractionation factor from Horita, 2014) in preglacial samples gives consistent temperatures (37 ± 4°C, 1 SD $n = 7$) assuming modern seawater δ^{18}O values and no polar ice (−1.2‰ VSMOW, Lear et al., 2000; Cramer et al., 2011; see Bergmann, al Balushi, et al., 2018; Bergmann, Finnegan, et al., 2018; and Henkes et al., 2018, for discussion of paleoseawater δ^{18}O values). Preglacial samples <50°C have fluid $\delta^{18}O_{VSMOW}$ values of +0.7‰ to +1.8‰ VSMOW (Figure 4); these higher fluid δ^{18}O values at elevated clumped isotope temperatures are consistent with rock-buffered cementation or dissolution and reprecipitation (e.g., Staudigel & Swart, 2019; Stolper et al., 2018). If preglacial dolomites precipitated from seawater with a $\delta^{18}O_{VSMOW}$ of −1.2‰, they would require a 16% contribution of dolomite precipitated during burial to account for observed clumped isotope temperatures assuming rock buffered alteration at a 122°C burial temperature; at 160°C, this contribution would be 12%. Source waters consistent with lower marine δ^{18}O values (e.g., Galili et al., 2019) or higher water/rock ratios for diagenesis would require proportionately greater degrees of burial alteration to explain the composition of the preglacial dolomites (Table 1). Alternatively, given the association of evaporite pseudomorphs and stromatolites in the preglacial facies association, it is also possible that fluid δ^{18}O values were higher from primary restriction and evaporative concentration in the depositional environment (e.g., McKenzie, 1981). If both glacial and

Table 1
Summary of Mineral $\delta^{18}O$, Temperature, and Initial Source Fluid $\delta^{18}O$ for Preglacial and Synglacial Dolomites

Data treatment	Strata	δ^{18O} mineral (‰ VPDB)	Temp (°C)	Initial fluid $\delta^{18}O$ (‰ VSMOW)	% equilibrated to burial estimate (122°)
Raw data	Preglacial	−1.5 (−2.2)	48 (53)	**+1.8 (+1.9)**	0%
Raw data	Glacial	+7.9 (+6.8)	19 (33)	**+4.8 (+6.9)**	0%
Preglacial fluid $\delta^{18}O$ −1.2‰	Preglacial	−1.5 (−2.2)	**34 (37)**	−1.2	**22% (23%)**
Preglacial fluid $\delta^{18}O$ −1.2‰	Glacial	+7.9 (+6.8)	**2 (16)**	**−0.1 (+2.8)**	22% (23%)
Preglacial fluid $\delta^{18}O$ −5‰	Preglacial	−1.5 (−2.2)	**18 (21)**	−5	**39% (41%)**
Preglacial fluid $\delta^{18}O$ −5‰	Glacial	+7.9 (+6.8)	**−16 (−2)**	**−6.3 (−2.8)**	39% (41%)
15% equilibrated	*Preglacial*	*−1.5 (−2.2)*	***39 (44)***	***−0.1 (0.2)***	*15%*
15% equilibrated	*Glacial*	*+7.9 (+6.8)*	***8 (23)***	***+1.8 (+4.5)***	*15%*
30% equilibrated	Preglacial	−1.5 (−2.2)	**27 (33)**	**−2.7 (−2.3)**	30.0%
30% equilibrated	Glacial	+7.9 (+6.8)	**−6 (10)**	**−2.6 (+0.9)**	30.0%

Note. Data are presented for the lowest sample temperatures associated in each climate state with mean values in parentheses. Raw data are transformed via possible rock-buffered alteration trajectories based on hypothetical initial source fluid $\delta^{18}O$ values or the percent of dolomite equilibrated to peak burial estimate. For each data treatment, the preglacial percent equilibrated is used to estimate the initial fluid $\delta^{18}O$ values for glacial conditions. In each row of the transformed data, $\delta^{18}O$ mineral is held constant, and the treatment is used to calculate either the percent equilibrated (with initial fluid assumed) or initial fluid composition (with percent equilibrated assumed). Calculated values are in bold, and rows containing the preferred interpretation are italicized. In all treatments, the difference in minimum temperatures between preglacial and glacial states is similar to that of the raw data.

preglacial facies experienced similar rock-buffered dissolution and reprecipitation, then the early temperature and source fluid $\delta^{18}O$ values for glacial dolomicrite may have also been lower than measured in this clumped isotope analysis.

For the lowest-temperature dolomicrite and soft sediment samples (19°C and 21°C, respectively), a hypothetical 15% contribution of dolomite that precipitated at 122°C burial temperatures (e.g., Table 1) would yield initial temperatures of +8°C and +10°C with reconstructed fluid $\delta^{18}O_{VSMOW}$ values of +1.8‰ and +4.5‰, respectively (Figure 6b). The reconstructed fluid $\delta^{18}O_{VSMOW}$ values are more positive than modern seawater, albeit with less extreme values than initially calculated from the clumped isotope thermometer (+4.8‰ and +7.7‰). Higher levels of rock-buffered alteration would correspond to lower initial temperatures and lower source fluid $\delta^{18}O$ estimates (Table 1).

High $\delta^{18}O$ values for early lithifying or diagenetic glacial fluids indicate either sequestration of precipitation in continental ice sheets (e.g., Raymo et al., 2018; Shackleton, 1967) or more local restriction and evaporation (e.g., Gat, 1995; Horita, 2008). The association of glacial dolomites with diamictite suggests the former likely dominates the signal. Evaporative enrichment of $^{18}O/^{16}O$ to the extent inferred from these dolomites relative to preglacial dolomites (approximately 3–5‰, Table 1) is at the upper end of enrichment observed in modern arid glacial environments (e.g., Gooseff et al., 2003; Matsubaya et al., 1979). Other mechanisms for concentrating solutes in glacial environments like freeze concentration (Staudigel et al., 2018) cannot explain the observed trends here, as freeze concentration is associated with lower fluid $\delta^{18}O$ values (Horita, 2008). Thus, transformed clumped isotope results assuming some component of carbonate precipitated during burial are broadly consistent with glacial conditions interpreted from carbonate facies.

4.5. Implications for Cryogenian Climate Reconstructions

The $\delta^{18}O$ composition and Δ_{47} temperature of Petrovbreen Member cold water carbonate beds constrains depositional and early diagenetic conditions at points within this Cryogenian glacial episode. An offset in minimum temperatures (29°C) between preglacial and glacial low-latitude carbonates is significantly more severe than reconstructed for Phanerozoic glaciations (Finnegan et al., 2011; Grossman et al., 2008; Raymo et al., 2018) and is more consistent with models for entering a Snowball Earth climate state with equatorial temperatures <0°C (Abbot et al., 2013; Pierrehumbert et al., 2011). The associated relative enrichment of water $\delta^{18}O_{VSMOW}$ values from preglacial to glacial carbonates is ~3–5‰, the lower end of which overlaps with the highest Phanerozoic estimates for glacial sequestration of water in ice sheets (e.g., Finnegan et al., 2011; Lea et al., 2000).

The dolomicrites analyzed in this study are uncommon in the Petrovbreen Member (Figure 1; Fairchild, 1983) and are not a common facies in other Cryogenian glacial sections (e.g., Spence et al., 2016; Spencer, 1971). Dolomicrites may reflect conditions particular to this glaciated carbonate platform with local

increases in alkalinity from glacial processing of detrital carbonate (cf. Fairchild et al., 2004). Stratigraphic relationships suggest that Petrovbreen Member dolomicrites do not represent deposition within the final deglaciation, as the diamictite successions in Svalbard are crosscut by sediment-filled wedges interpreted as periglacial exposure surfaces (Fairchild et al., 1989). Such exposure surfaces require progressive fall in base level or sublimation, possibly indicating ice sheet expansion following dolomicrite deposition. It is thus possible that these carbonates do not capture the coldest Snowball Earth conditions. Carbonates from the overlying Marinoan glaciation in Svalbard are similarly interpreted to have formed outside of the coldest part of the glacial episode; in that case carbonates are consistent with precipitation late in the glaciation (Bao et al., 2009; Benn et al., 2015; Fairchild, Fleming, et al., 2016).

The partial preservation of clumped isotope signatures through stratigraphic changes in climate bolsters confidence in a depositional or early diagenetic source for δ^{18}O and δ^{13}C isotopic records preserved in these carbonates (e.g., Halverson et al., 2018; Hoffman et al., 2012), rather than being exclusively a product of deep burial. Judicious application of carbonate clumped isotope thermometry in other well-preserved Neoproterozoic strata may continue to inform climate and seawater evolution through the environmental perturbations of the era.

5. Conclusions

The Neoproterozoic Elbobreen Formation of NE Svalbard contains carbonate-rich facies preceding and coincident with the first Cryogenian Snowball Earth episode. These carbonates preserve shifts in δ^{18}O and Δ_{47} temperature alongside sedimentological evidence of environmental change; Δ_{47} temperatures presented here are the first documented from Snowball Earth synglacial carbonates. Calcite clumped isotope temperatures have likely experienced partial solid-state reordering during burial. Dolomite clumped isotope temperatures are warmer than expected for analogous modern depositional environments, likely resulting from dolomite lithification, dissolution and reprecipitation during burial or partial solid-state reordering. Despite warm preglacial temperatures, minimum and mean temperatures for fabric retentive glacial dolomite facies are 29°C and 26 ± 10°C (95% CL) colder than preglacial facies, respectively. Detrital dolomitic clasts from within the glacial diamictites also yield clumped isotope temperatures and mineral δ^{18}O values distinct from their matrix, passing an isotope conglomerate test. When combined with stratigraphic and petrographic context, geochemical records indicate that many carbonates followed a rock-buffered diagenetic pathway, indicating that δ^{18}O compositions are retained. Reconstructed precipitating fluid $\delta^{18}O_{VSMOW}$ values for the glacial facies are enriched by 3–5‰ compared to preglacial facies. Temperature changes and higher fluid δ^{18}O values are consistent with a dramatic cooling associated with glaciation, the growth of ice sheets, and concurrent enrichment of the marine reservoir. The 20–30°C shift in Δ_{47} temperatures observed between glacial and preglacial carbonates far exceeds cooling documented in more recent Phanerozoic glaciations (e.g., Brenchley et al., 1994; Montañez & Poulsen, 2013) and attests to distinctive climate dynamics in this Neoproterozoic Snowball Earth episode.

Conflict of Interest

The authors declare no conflicts of interest relevant to this study.

Data Availability Statement

All data used in this study are available in this article and its supporting information. Processed data from carbonate clumped isotope analyses are available as supporting information and raw data are submitted to the EARTHCHEM Database (https://doi.org/10.26022/IEDA/111534).

Acknowledgments

We thank A. Knoll for his insights into Svalbard carbonate stratigraphy and discussion of promising field localities. Field work in 2014 was supported by the Harvard Society of Fellows and the Milton Fund at Harvard University; J. Cooper assisted in collecting and documenting samples. Discussions with I. Fairchild and his contribution of additional samples improved this study. G. Halverson, J. Strauss, and N. Tosca further informed our work through their helpful discussions. We would also like to thank M. Bonifacie, L. Derry, anonymous reviewers, Editor P. Zeitler, and Bergmann lab members M. Cantine, J. Wilcots, and S. Goldberg for comments and suggestions on earlier drafts of this manuscript. T. J. M. was supported by an Agouron Institute Postdoctoral Fellowship. K. Bergmann acknowledges support for laboratory expenses from the MIT Node of the NASA Astrobiology Institute, NASA Exobiology Grant 80NSSC19K0464 and the MIT Wade Fund and the Packard Foundation. Research was conducted and permitted under the Research in Svalbard (RIS) ID 6867.

References

Abbot, D. S., Voigt, A., Li, D., Hir, G. L., Pierrehumbert, R. T., Branson, M., et al. (2013). Robust elements of Snowball Earth atmospheric circulation and oases for life. *Journal of Geophysical Research: Atmospheres*, *118*, 6017–6027. https://doi.org/10.1002/jgrd.50540

Bao, H., Fairchild, I. J., Wynn, P. M., & Spötl, C. (2009). Stretching the envelope of past surface environments: Neoproterozoic glacial lakes from Svalbard. *Science (New York, N.Y.)*, *323*(5910), 119–122. https://doi.org/10.1126/science.1165373

Benn, D. I., le Hir, G., Bao, H., Donnadieu, Y., Dumas, C., Fleming, E. J., et al. (2015). Orbitally forced ice sheet fluctuations during the Marinoan Snowball Earth glaciation. *Nature Geoscience*, *8*(9), 704–707. https://doi.org/10.1038/ngeo2502

Bergmann, K. D., al Balushi, S. A. K., Mackey, T. J., Grotzinger, J. P., & Eiler, J. M. (2018). A 600-million-year carbonate clumped-isotope record from the sultanate of Oman. *Journal of Sedimentary Research*, *88*(8), 960–979. https://doi.org/10.2110/jsr.2018.51

Bergmann, K. D., Finnegan, S., Creel, R., Eiler, J. M., Hughes, N. C., Popov, L. E., & Fischer, W. W. (2018). A paired apatite and calcite clumped isotope thermometry approach to estimating Cambro-Ordovician seawater temperatures and isotopic composition. *Geochimica et Cosmochimica Acta*, *224*, 18–41. https://doi.org/10.1016/J.GCA.2017.11.015

Bergström, S. M. (1980). Conodonts as paleotemperature tools in Ordovician rocks of the Caledonides and adjacent areas in Scandinavia and the British Isles. *Geologiska Föreningens i Stockholm Förhandlingar*, *102*(4), 377–392. https://doi.org/10.1103/PhysRevLett.101.105501

Bernasconi, S. M., Müller, I. A., Bergmann, K. D., Breitenbach, S. F. M., Fernandez, A., Hodell, D. A., et al. (2018). Reducing uncertainties in carbonate clumped isotope analysis through consistent carbonate-based standardization. *Geochemistry, Geophysics, Geosystems*, *19*, 2895–2914. https://doi.org/10.1029/2017GC007385

Bonifacie, M., Calmels, D., Eiler, J. M., Horita, J., Chaduteau, C., Vasconcelos, C., et al. (2017). Calibration of the dolomite clumped isotope thermometer from 25 to 350°C, and implications for a universal calibration for all (Ca, Mg, Fe) CO_3 carbonates. *Geochimica et Cosmochimica Acta*, *200*, 255–279. https://doi.org/10.1016/j.gca.2016.11.028

Brenchley, P. J., Marshall, J. D., Carden, G. A. F., Robertson, D. B. R., Long, D. G. F., Meidla, T., et al. (1994). Bathymetric and isotopic evidence for a short-lived Late Ordovician glaciation in a greenhouse period. *Geology*, *22*(4), 295–298. https://doi.org/10.1130/0091-7613(1994)022<0295:BAIEFA>2.3.CO;2

Budd, D. A. (1989). Micro-rhombic calcite and microporosity in limestones: A geochemical study of the lower cretaceous thamama group, U.A.E. *Sedimentary Geology*, *63*(3–4), 293–311. https://doi.org/10.1016/0037-0738(89)90137-1

Cohen, P. A., & Riedman, L. A. (2018). It's a protist-eat-protist world: Recalcitrance, predation, and evolution in the Tonian-Cryogenian ocean. *Emerging Topics in Life Sciences*, *2*(2), 173–180. https://doi.org/10.1042/ETLS20170145

Cramer, B. S., Miller, K. G., Barrett, P. J., & Wright, J. D. (2011). Late Cretaceous-Neogene trends in deep ocean temperature and continental ice volume: Reconciling records of benthic foraminiferal geochemistry ($\delta^{18}O$ and Mg/Ca) with sea level history. *Journal of Geophysical Research*, *116*, C12023. https://doi.org/10.1029/2011JC007255

Creveling, J. R., & Mitrovica, J. X. (2014). The sea-level fingerprint of a Snowball Earth deglaciation. *Earth and Planetary Science Letters*, *399*, 74–85. https://doi.org/10.1016/j.epsl.2014.04.029

Cummins, R. C., Finnegan, S., Fike, D. A., Eiler, J. M., & Fischer, W. W. (2014). Carbonate clumped isotope constraints on Silurian ocean temperature and seawater $\delta^{18}O$. *Geochimica et Cosmochimica Acta*, *140*, 241–258. https://doi.org/10.1016/j.gca.2014.05.024

Daëron, M., Blamart, D., Peral, M., & Affek, H. P. (2016). Absolute isotopic abundance ratios and the accuracy of Δ_{47} measurements. *Chemical Geology*, *442*, 83–96. https://doi.org/10.1016/J.CHEMGEO.2016.08.014

Defliese, W. F., Hren, M. T., & Lohmann, K. C. (2015). Compositional and temperature effects of phosphoric acid fractionation on Δ_{47} analysis and implications for discrepant calibrations. *Chemical Geology*, *396*, 51–60. https://doi.org/10.1016/j.chemgeo.2014.12.018

Dennis, K. J., Affek, H. P., Passey, B. H., Schrag, D. P., & Eiler, J. M. (2011). Defining an absolute reference frame for 'clumped'isotope studies of CO2. *Geochimica et Cosmochimica Acta*, *75*(22), 7117–7131. https://doi.org/10.1016/j.gca.2011.09.025

Dickson, J. A. D., & Coleman, M. L. (1980). Changes in carbon and oxygen isotope composition during limestone diagenesis. *Sedimentology*, *27*, 107–118. https://doi.org/10.1002/9781444304510.ch21

Dörr, N., Lisker, F., Clift, P. D., Carter, A., Gee, D. G., Tebenkov, A. M., & Spiegel, C. (2012). Late Mesozoic-Cenozoic exhumation history of northern Svalbard and its regional significance: Constraints from apatite fission track analysis. *Tectonophysics*, *514–517*, 81–92. https://doi.org/10.1016/j.tecto.2011.10.007

Dörr, N., Lisker, F., Piepjohn, K., & Spiegel, C. (2019). Cenozoic development of northern Svalbard based on thermochronological data. *Terra Nova*, *31*(3), 306–315. https://doi.org/10.1111/ter.12402

Eggins, S., de Deckker, P., & Marshall, J. (2003). Mg/Ca variation in planktonic foraminifera tests: Implications for reconstructing palaeo-seawater temperature and habitat migration. *Earth and Planetary Science Letters*, *212*(3–4), 291–306. https://doi.org/10.1016/S0012-821X(03)00283-8

Eiler, J. M. (2007). "Clumped-isotope" geochemistry—The study of naturally-occurring, multiply-substituted isotopologues. *Earth and Planetary Science Letters*, *262*(3–4), 309–327. https://doi.org/10.1016/j.epsl.2007.08.020

Eiler, J. M. (2011). Paleoclimate reconstruction using carbonate clumped isotope thermometry. *Quaternary Science Reviews*, *30*, 3575–3588. https://doi.org/10.1016/j.quascirev.2011.09.001

Epstein, A. G., Epstein, J. B., & Harris, L. D. (1977). Conodont color alteration—An index to organic metamorphism. *USGS Professional Paper*, *995*, 27. https://doi.org/10.3133/pp995

Evans, D., Sagoo, N., Renema, W., Cotton, L. J., Müller, W., Todd, J. A., et al. (2018). Eocene greenhouse climate revealed by coupled clumped isotope-Mg/Ca thermometry. *Proceedings of the National Academy of Sciences of the United States of America*, *115*(6), 1174–1179. https://doi.org/10.1073/pnas.1714744115

Ewing, R. C., Eisenman, I., Lamb, M. P., Poppick, L., Maloof, A. C., & Fischer, W. W. (2014). New constraints on equatorial temperatures during a Late Neoproterozoic snowball Earth glaciation. *Earth and Planetary Science Letters*, *406*, 110–122. https://doi.org/10.1016/j.epsl.2014.09.017

Fairchild, I. J., Hambrey, M. J., Spiro, B., & Jefferson, T. H. (1989). Late Proterozoic glacial carbonates in northeast Spitsbergen: New insights into the carbonate–tillite association. *Geological Magazine*, *126*(05), 469–490.

Fairchild, I. J. (1983). Effects of glacial transport and neomorphism on Precambrian dolomite crystal sizes. *Nature*, *304*(August), 714–716.

Fairchild, I. J., Bonnand, P., Davies, T., Fleming, E. J., Grassineau, N., Halverson, G. P., et al. (2016). The Late Cryogenian Warm Interval, NE Svalbard: Chemostratigraphy and genesis. *Precambrian Research*, *281*, 128–154. https://doi.org/10.1016/j.precamres.2016.05.013

Fairchild, I. J., Bradby, L., & Spiro, B. (2004). Reactive carbonate in glacial systems: A preliminary synthesis of its creation, dissolution and reincarnation. In M. Deynoux, J. M. G. Miller, & E. W. Domack (Eds.), *Earth's glacial record* (pp. 176–192). Cambridge: Cambridge University Press.

Fairchild, I. J., Fleming, E. J., Bao, H., Benn, D. I., Boomer, I., Dublyansky, Y. V., et al. (2016). Continental carbonate facies of a Neoproterozoic panglaciation, north-east Svalbard. *Sedimentology*, *63*(2), 443–497. https://doi.org/10.1111/sed.12252

Fairchild, I. J., & Hambrey, M. J. (1984). The Vendian succession of northeastern Spitsbergen: Petrogenesis of a dolomite-tillite association. *Precambrian Research*, *26*(2), 111–167. https://doi.org/10.1016/0301-9268(84)90042-1

Fairchild, I. J., Spencer, A. M., Ali, D. O., Anderson, R. P., Anderton, R., Boomer, I., et al. (2017). Tonian-Cryogenian boundary sections of Argyll, Scotland. *Precambrian Research*, *319*, 37–64. https://doi.org/10.1016/J.PRECAMRES.2017.09.020

Fernandez, A., Muller, I. A., Rodriguez-Sanz, L., van Dijk, J., Looser, N., & Bernasconi, S. M. (2017). A reassessment of the precision of carbonate clumped isotope measurements: Implications for calibrations and paleoclimate reconstructions. *Geochemistry, Geophysics, Geosystems*, *18*, 4375–4386. https://doi.org/10.1002/2017GC007106

Ferry, J. M., Passey, B. H., Vasconcelos, C., & Eiler, J. M. (2011). Formation of dolomite at 40–80°C in the Latemar carbonate buildup, Dolomites, Italy, from clumped isotope thermometry. *Geology*, *39*(6), 571–574. https://doi.org/10.1130/G31845.1

Finnegan, S., Bergmann, K., Eiler, J. M., Jones, D. S., Fike, D. A., Eisenman, I., et al. (2011). The magnitude and duration of Late Ordovician-Early Silurian glaciation. *Science (New York, N.Y.)*, *331*(6019), 903–906. https://doi.org/10.1126/science.1200803

Flügel, E. (2004). *Microfacies of carbonate rocks: Analysis, interpretation and application* (p. 976). Berlin, New York: Springer. ISBN: 9783540220169. https://doi.org/10.1007/978-3-642-03796-2

Galili, N., Shemesh, A., Yam, R., Brailovsky, I., Sela-Adler, M., Schuster, E. M., et al. (2019). The geological history of seawater oxygen isotopes from marine iron oxides. *Science*, *473*(August), 469–473.

Gasser, D. (2014). The Caledonides of Greenland, Svalbard and other Arctic areas: Status of research and open questions. In F. Corfu, D. Gasser, & D. M. Chew (Eds.), *New perspectives on the Caledonides of Scandinavia and related areas* (pp. 93–129). London, Special Publications: Geological Society. https://doi.org/10.1144/SP390.17

Gat, J. R. (1995). Stable Isotopes of Fresh and Saline Lakes. In A. Lerman, D. M. Imboden, & J. R. Gat (Eds.), *Physics and chemistry of lakes* (pp. 139–165). New York: Springer-Verlag.

Ghosh, P., Adkins, J., Affek, H., Balta, B., Guo, W., Schauble, E. A., et al. (2006). ^{13}C-^{18}O bonds in carbonate minerals: A new kind of paleothermometer. *Geochimica et Cosmochimica Acta*, *70*(6), 1439–1456. https://doi.org/10.1016/j.gca.2005.11.014

Gilbert, P. U. P. A., Bergmann, K. D., Myers, C. E., Marcus, M. A., DeVol, R. T., Sun, C. Y., et al. (2017). Nacre tablet thickness records formation temperature in modern and fossil shells. *Earth and Planetary Science Letters*, *460*, 281–292. https://doi.org/10.1016/j.epsl.2016.11.012

Gooseff, M. N., Mcknight, D. M., Runkel, R. L., & Vaughn, B. H. (2003). Determining long time-scale hyporheic zone flow paths in. *Antarctic streams*, *17*, 1691–1710. https://doi.org/10.1002/hyp.1210

Grossman, E. L., Yancey, T. E., Jones, T. E., Bruckschen, P., Chuvashov, B., Mazzullo, S. J., & Mii, H.-S. (2008). Glaciation, aridification, and carbon sequestration in the Permo-Carboniferous: The isotopic record from low latitudes. *Palaeogeography, Palaeoclimatology, Palaeoecology*, *268*(3–4), 222–233. https://doi.org/10.1016/j.palaeo.2008.03.053

Halverson, G. P., Kunzmann, M., Strauss, J. V., & Maloof, A. C. (2018). The Tonian-Cryogenian transition in Northeastern Svalbard. *Precambrian Research*, *319*, 79–95. https://doi.org/10.1016/J.PRECAMRES.2017.12.010

Halverson, G. P., Maloof, A. C., & Hoffman, P. F. (2004). The Marinoan glaciation (Neoproterozoic) in northeast Svalbard. *Basin Research*, *16*, 297–324. https://doi.org/10.1111/j.1365-2117.2004.00234.x

Halverson, G. P. (2003). Towards an integrated stratigraphic and carbon isotopic record for the Neoproterozoic. Department of Earth and Planetary Sciences. Harvard University.

Halverson, G. P., Hoffman, P. F., Schrag, D. P., Maloof, A. C., & Rice, A. H. N. (2005). Toward a Neoproterozoic composite carbon-isotope record. *Geological Society of America Bulletin*, *117*(9), 1181. https://doi.org/10.1130/b25630.1

Halverson, G. P., Maloof, A. C., Schrag, D. P., Dudás, F. Ö., & Hurtgen, M. (2007). Stratigraphy and geochemistry of a ca 800 Ma negative carbon isotope interval in northeastern Svalbard. *Chemical Geology*, *237*(1–2), 5–27. https://doi.org/10.1016/j.chemgeo.2006.06.013

Hambrey, M. J. (1982). Late Precambrian diamictites of northeastern Svalbard. *Geological Magazine*, *119*(06), 527. https://doi.org/10.1017/S0016756800027035

Harland, W. B., Wallis, R. H., & Gayer, R. A. (1966). A revision of the lower Hecla Hoek succession in central north Spitsbergen and correlation elsewhere. *Geological Magazine*, *103*(01), 70. https://doi.org/10.1017/S0016756800050433

Henkes, G. A., Passey, B. H., Grossman, E. L., Shenton, B. J., Pérez-Huerta, A., & Yancey, T. E. (2014). Temperature limits for preservation of primary calcite clumped isotope paleotemperatures. *Geochimica et Cosmochimica Acta*, *139*, 362–382. https://doi.org/10.1016/J.GCA.2014.04.040

Henkes, G. A., Passey, B. H., Grossman, E. L., Shenton, B. J., Yancey, T. E., & Perez-Huerta, A. (2017). Temperature evolution and the oxygen isotope composition of Phanerozoic oceans from carbonate clumped isotope thermometry. *Planetary Science Letters*, *490*, 40–50. https://doi.org/10.1016/j.epsl.2018.02.001

Henkes, G. A., Passey, B. H., Grossman, E. L., Shenton, B. J., Yancey, T. E., & Pérez-Huerta, A. (2018). Temperature evolution and the oxygen isotope composition of Phanerozoic oceans from carbonate clumped isotope thermometry. *Earth and Planetary Science Letters*, *490*, 40–50. https://doi.org/10.1016/J.EPSL.2018.02.001

Hoffman, P. F. (2009). Pan-glacial—A third state in the climate system. *Geology Today*, *25*(3), 100–107. https://doi.org/10.1111/j.1365-2451.2009.00716.x

Hoffman, P. F., Abbot, D. S., Ashkenazy, Y., Benn, D. I., Brocks, J. J., Cohen, P. A., et al. (2017). Snowball Earth climate dynamics and Cryogenian geology-geobiology. *Science Advances*, *3*(11), e1600983. https://doi.org/10.1126/sciadv.1600983

Hoffman, P. F., Halverson, G. P., Domack, E. W., Maloof, A. C., Swanson-hysell, N. L., & Cox, G. M. (2012). Cryogenian glaciations on the southern tropical paleomargin of Laurentia (NE Svalbard and East Greenland), and a primary origin for the upper Russøya (Islay) carbon isotope excursion. *Precambrian Research*, *206–207*, 137–158. https://doi.org/10.1016/j.precamres.2012.02.018

Hoffman, P. F., Kaufman, A. J., Halverson, G. P., & Schrag, D. P. (1998). A Neoproterozoic Snowball Earth. *Science (New York, N.Y.)*, *281*(5381), 1342–1346. https://doi.org/10.1126/SCIENCE.281.5381.1342

Hood, A. V. S., Wallace, M. W., & Drysdale, R. N. (2011). Neoproterozoic aragonite-dolomite seas? Widespread marine dolomite precipitation in Cryogenian reef complexes. *Geology*, *39*(9), 871–874. https://doi.org/10.1130/G32119.1

Horita, J. (2008). Isotopic evolution of saline lakes in the low-latitude and polar regions. *Aquatic Geochemistry*, *15*(1–2), 43–69. https://doi.org/10.1007/s10498-008-9,050-3

Horita, J. (2014). Oxygen and carbon isotope fractionation in the system dolomite-water-CO_2 to elevated temperatures. *Geochimica et Cosmochimica Acta*, *129*, 111–124. https://doi.org/10.1016/j.gca.2013.12.027

Huntington, K. W., Budd, D. A., Wernicke, B. P., & Eiler, J. M. (2011). Use of clumped-isotope thermometry to constrain the crystallization temperature of diagenetic calcite. *Journal of Sedimentary Research*, *81*(9), 656–669. https://doi.org/10.2110/jsr.2011.51

Hyde, W. T., Crowley, T. J., Baum, S. K., & Peltier, W. R. (2000). Neoproterozoic "snowball Earth" simulations with a coupled climate/ice-sheet model. *Nature*, *405*(6785), 425–429. https://doi.org/10.1038/35013005

Jaffrés, J. B. D., Shields, G. A., & Wallmann, K. (2007). The oxygen isotope evolution of seawater: A critical review of a long-standing controversy and an improved geological water cycle model for the past 3.4 billion years. *Earth-Science Reviews*, *83*(1–2), 83–122. https://doi.org/10.1016/j.earscirev.2007.04.002

Jean-Baptiste, P., Charlou, J. L., & Stievenard, M. (1997). Oxygen isotope study of mid-ocean ridge hydrothermal fluids: Implication for the oxygen-18 budget of the oceans. *Geochimica et Cosmochimica Acta*, *61*(13), 2,669–2,677. https://doi.org/10.1016/S0016-7037(97)00090-2

Jennings, J., Ruppel, S. C., & Ward, W. B. (2000). Geostatistical analysis of permeability data and modeling of fluid-flow effects in carbonate outcrops. *SPE Reservoir Evaluation and Engineering*, *3*(4), 292–303. https://doi.org/10.2118/65370-pa

John, C. M., & Bowen, D. (2016). Community software for challenging isotope analysis: First applications of 'Easotope' to clumped isotopes. *Rapid Communications in Mass Spectrometry*, *30*(21), 2,285–2,300. https://doi.org/10.1002/rcm.7720

Kasting, J. F., Howard, M. T., Wallmann, K., Veizer, J., Shields, G., & Jaffrs, J. (2006). Paleoclimates, ocean depth, and the oxygen isotopic composition of seawater. *Earth and Planetary Science Letters*, *252*(1–2), 82–93. https://doi.org/10.1016/j.epsl.2006.09.029

Kelson, J. R., Huntington, K. W., Schauer, A. J., Saenger, C., & Lechler, A. R. (2017). Toward a universal carbonate clumped isotope calibration: Diverse synthesis and preparatory methods suggest a single temperature relationship. *Geochimica et Cosmochimica Acta*, *197*, 104–131. https://doi.org/10.1016/J.GCA.2016.10.010

Kim, J. H., Schouten, S., Hopmans, E. C., Donner, B., & Sinninghe Damsté, J. S. (2008). Global sediment core-top calibration of the TEX86 paleothermometer in the ocean. *Geochimica et Cosmochimica Acta*, *72*(4), 1154–1173. https://doi.org/10.1016/j.gca.2007.12.010

Kim, S.-T., & O'Neil, J. R. (1997). Equilibrium and nonequilibrium oxygen isotope effects in synthetic carbonates. *Geochimica et Cosmochimica Acta*, *61*(16), 3461–3475. https://doi.org/10.1016/S0016-7037(97)00169-5

Kirschvink, J. L. (1992). Late Proterozoic low-latitude global glaciation: The Snowball Earth. The Proterozoic biosphere : A multidisciplinary study (pp. 51–52). New York: Cambridge University Press. ISBN 9780521366151. Retrieved from https://authors.library.caltech.edu/36446/1/Kirschvink_1992p51.pdf

Knauth, L. P., & Kennedy, M. J. (2009). The late Precambrian greening of the Earth. *Nature*, *460*(7256), 728–732. https://doi.org/10.1038/nature08213

Knoll, A. H., & Calder, S. (1983). Microbiotas of the Late Precambrian Rysso Formation, Nordaustlandet, Svalbard. *Paleontology*, *26*(3), 467–496. Retrieved from. https://cdn.palass.org/publications/palaeontology/volume_26/pdf/vol26_part3_pp467-496.pdf

Knoll, A. H., & Swett, K. (1990). Carbonate deposition during the late Proterozoic Era: An example from Spitsbergen. *American Journal of Science*, *290A*, 104–132.

Kupecz, J. A., Montanez, I. P., & Gao, G. (1993). Recrystallization of dolomite with time. In R. Rezak, & D. L. Lavoie (Eds.), *Carbonate microfabrics* (pp. 187–193). New York, NY: Springer New York. https://doi.org/10.1007/978-1-4,684-9,421-1_14

Lacroix, B., & Niemi, N. A. (2019). Investigating the effect of burial histories on the clumped isotope thermometer: An example from the Green River and Washakie Basins, Wyoming. *Geochimica et Cosmochimica Acta*, *247*, 40–58. https://doi.org/10.1016/J.GCA.2018.12.016

Lea, D. W., Pak, D. K., & Spero, H. J. (2000). Climate impact of late Quaternary equatorial Pacific sea surface temperature variations. *Science*, *289*(5485), 1719–1724. https://doi.org/10.1126/science.289.5485.1719

Lear, C. H., Elderfield, H., & Wilson, P. A. (2000). Cenozoic deep-sea temperatures and global ice volumes from Mg/Ca in benthic foraminiferal calcite. *Science*, *287*(5451), 269–272. https://doi.org/10.1126/science.287.5451.269

Lee, C., Love, G. D., Hopkins, M. J., Kröger, B., Franeck, F., & Finnegan, S. (2019). Lipid biomarker and stable isotopic profiles through Early-Middle Ordovician carbonates from Spitsbergen, Norway. *Organic Geochemistry*, *131*, 5–18. https://doi.org/10.1016/j.orggeochem.2019.02.008

Lehnert, O., Stouge, S., & Brandl, P. A. (2013). Conodont biostratigraphy in the Early to Middle Ordovician strata of the Oslobreen Group in Ny Friesland, Svalbard. *Zeitschrift der Deutschen Gesellschaft für Geowissenschaften*, *164*(January), 149–172. https://doi.org/10.1127/1860-1804/2013/0003

Lloyd, M. K., Ryb, U., & Eiler, J. M. (2018). Experimental calibration of clumped isotope reodering in dolomite. *Geochimica et Cosmochimica Acta*, *242*, 1–20. https://doi.org/10.1016/J.GCA.2018.08.036

Lohmann, K. C. (1988). Geochemical patterns of meteoric diagenetic systems and their application to studies of paleokarst. In N. P. James, & P. W. Choquette (Eds.), *Paleokarst* (pp. 58–80). New York, NY: Springer New York. https://doi.org/10.1007/978-1-4,612-3,748-8_3

Macdonald, F. A., Schmitz, M. D., Crowley, J. L., Roots, C. F., Jones, D. S., Maloof, A. C., et al. (2010). Calibrating the Cryogenian. *Science*, *327*(5970), 1241–1243. https://doi.org/10.1126/science.1183325

MacLennan, S., Park, Y., Swanson-Hysell, N., Maloof, A., Schoene, B., Gebreslassie, M., et al. (2018). The arc of the Snowball: U-Pb dates constrain the Islay anomaly and the initiation of the Sturtian glaciation. *Geology*, *46*(6), 539–542. https://doi.org/10.1130/G40171.1

Maloof, A. C., Halverson, G. P., Kirschvink, J. L., Schrag, D. P., Weiss, B. P., & Hoffman, P. F. (2006). Combined paleomagnetic, isotopic, and stratigraphic evidence for true polar wander from the Neoproterozoic Akademikerbreen Group, Svalbard, Norway. *Geological Society of America Bulletin*, *118*(9–10), 1099–1124. https://doi.org/10.1130/B25892.1

Mangenot, X., Gasparrini, M., Rouchon, V., & Bonifacie, M. (2018). Basin-scale thermal and fluid flow histories revealed by carbonate clumped isotopes (Δ_{47})—Middle Jurassic carbonates of the Paris Basin depocentre. *Sedimentology*, *65*(1), 123–150. https://doi.org/10.1111/sed.12427

Matsubaya, O., Sakai, H., Torii, T., Burton, H. H., & Kerry, K. (1979). Antarctic saline lakes—Stable isotopic ratios, chemical compositions and evolution. *Geochemica et Cosmochimica Acta*, *43*, 7–25.

McKenzie, J. A. (1981). Holocene dolomitization of calcium carbonate sediments from the coastal sabkhas of Abu Dhabi, U.A.E.: A stable isotope study. *Holocene*, *89*(2), 185–198.

Montañez, I. P., & Poulsen, C. J. (2013). The Late Paleozoic ice age: An evolving paradigm. *Annual Review of Earth and Planetary Sciences*, *41*(1), 629–656. https://doi.org/10.1146/annurev.earth.031208.100118

Moore, C. (1989). *Carbonate diagenesis and porosity*, *Developments in Sedimentology* (Vol. 46, pp. 1–337). Amsterdam: Elsevier Science B.V.

Moshier, S. O. (1989). Microporosity in micritic limestones: a review. *Sedimentary Geology*, *63*(3–4), 191–213. https://doi.org/10.1016/0037-0738(89)90132-2

Müller, I. A., Rodriguez-Blanco, J. D., Storck, J. C., do Nascimento, G. S., Bontognali, T. R. R., Vasconcelos, C., et al. (2019). Calibration of the oxygen and clumped isotope thermometers for (proto-)dolomite based on synthetic and natural carbonates. *Chemical Geology*, *525*, 1–17. https://doi.org/10.1016/J.CHEMGEO.2019.07.014

Müller, I. A., Violay, M. E. S., Storck, J. C., Fernandez, A., van Dijk, J., Madonna, C., & Bernasconi, S. M. (2017). Clumped isotope fractionation during phosphoric acid digestion of carbonates at 70°C. *Chemical Geology*, *449*, 1–14. https://doi.org/10.1016/j.chemgeo.2016.11.030

Myers, C. E., Bergmann, K. D., Sun, C. Y., Boekelheide, N., Knoll, A. H., & Gilbert, P. U. P. A. (2018). Exceptional preservation of organic matrix and shell microstructure in a Late Cretaceous Pinna fossil revealed by photoemission electron spectromicroscopy. *Geology*, *46*(8), 711–714. https://doi.org/10.1130/G45271.1

Naylor, H. N., Defliese, W. F., Grossman, E. L., & Maupin, C. R. (2019). Investigation of the thermal history of the Delaware Basin (West Texas, USA) using carbonate clumped isotope thermometry. *Basin Research*, bre.12419. https://doi.org/10.1111/bre.12419

Passey, B. H., & Henkes, G. A. (2012). Carbonate clumped isotope bond reordering and geospeedometry. *Earth and Planetary Science Letters*, *351–352*, 223–236. https://doi.org/10.1016/j.epsl.2012.07.021

Peters, K. E., Walters, C. C., & Moldowan, J. M. (2005). Origin and Preservation of Organic Matter. *The biomarker guide* (Vol. 1, 2nd ed., pp. 3–17). Cambridge: Cambridge University Press.

Petersen, S. V., Defliese, W. F., Saenger, C., Daëron, M., Huntington, K. W., John, C. M., et al. (2019). Effects of improved ^{17}O correction on interlaboratory agreement in clumped isotope calibrations, estimates of mineral-specific offsets, and temperature dependence of acid digestion fractionation. *Geochemistry, Geophysics, Geosystems*, *20*(7), 3495–3519. https://doi.org/10.1029/2018GC008127

Pierrehumbert, R. T., Abbot, D. S., Voigt, A., & Koll, D. (2011). Climate of the Neoproterozoic. *Annual Review of Earth and Planetary Sciences*, *39*(1), 417–460. https://doi.org/10.1146/annurev-earth-040809-152447

Raymo, M. E., Kozdon, R., Evans, D., Lisiecki, L., & Ford, H. L. (2018). The accuracy of mid-Pliocene $\delta^{18}O$-based ice volume and sea level reconstructions. *Earth-Science Reviews*, *177*, 291–302. https://doi.org/10.1016/J.EARSCIREV.2017.11.022

Rooney, A. D., Strauss, J. V., Brandon, A. D., & Macdonald, F. A. (2015). A Cryogenian chronology: Two long-lasting synchronous Neoproterozoic glaciations. *Geology*, *43*(5), 459–462. https://doi.org/10.1130/G36511.1

Ryb, U., & Eiler, J. M. (2018). Oxygen isotope composition of the Phanerozoic ocean and a possible solution to the dolomite problem. *Proceedings of the National Academy of Sciences of the United States of America*, *115*(26), 6602–6607. https://doi.org/10.1073/pnas.1719681115

Schauer, A. J., Kelson, J., Saenger, C., & Huntington, K. W. (2016). Choice of ^{17}O correction affects clumped isotope (Δ_{47}) values of CO_2 measured with mass spectrometry. *Rapid Communications in Mass Spectrometry*, *30*(24), 2607–2616. https://doi.org/10.1002/rcm.7743

Shackleton, N. (1967). Oxygen isotope analyses and Pleistocene temperatures re-assessed. *Nature*, *215*(5096), 15–17. https://doi.org/10.1038/215015a0

Shuster, A. M., Wallace, M. W., van Smeerdijk Hood, A., & Jiang, G. (2018). The Tonian Beck Spring Dolomite: Marine dolomitization in a shallow, anoxic sea. *Sedimentary Geology*, *368*, 83–104. https://doi.org/10.1016/J.SEDGEO.2018.03.003

Spence, G. H., Le Heron, D. P., & Fairchild, I. J. (2016). Sedimentological perspectives on climatic, atmospheric and environmental change in the Neoproterozoic Era. *Sedimentology*, *63*(2), 253–306. https://doi.org/10.1111/sed.12261

Spencer, A. M. (1971). Late Pre-cambrian glaciation in Scotland. *Geological Society Memoir*, *6*(1), 5–102. https://doi.org/10.1144/GSL.MEM.1971.006.01.02

Staudigel, P. T., Murray, S., Dunham, D. P., Frank, T. D., Fielding, C. R., & Swart, P. K. (2018). Cryogenic brines as diagenetic fluids: Reconstructing the diagenetic history of the Victoria Land Basin using clumped isotopes. *Geochimica et Cosmochimica Acta*, *224*, 154–170. https://doi.org/10.1016/J.GCA.2018.01.002

Staudigel, P. T., & Swart, P. K. (2019). A diagenetic origin for isotopic variability of sediments deposited on the margin of Great Bahama Bank, insights from clumped isotopes. *Geochimica et Cosmochimica Acta*, *258*, 97–119. https://doi.org/10.1016/j.gca.2019.05.002

Stolper, D. A., & Eiler, J. M. (2015). The kinetics of solid-state isotope-exchange reactions for clumped isotopes: A study of inorganic calcites and apatites from natural and experimental samples. *American Journal of Science*, *315*(5), 363–411. https://doi.org/10.2475/05.2015.01

Stolper, D. A., Eiler, J. M., & Higgins, J. A. (2018). Modeling the effects of diagenesis on carbonate clumped-isotope values in deep- and shallow-water settings. *Geochimica et Cosmochimica Acta*, *227*, 264–291. https://doi.org/10.1016/J.GCA.2018.01.037

Strauss, J. V., Rooney, A. D., Macdonald, F. A., Brandon, A. D., & Knoll, A. H. (2014). 740 Ma vase-shaped microfossils from Yukon, Canada: Implications for Neoproterozoic chronology and biostratigraphy. *Geology*, *42*(8), 659–662. https://doi.org/10.1130/G35736.1

Swart, P. K., & Kennedy, M. J. (2012). Does the global stratigraphic reproducibility of $\delta^{13}C$ in neoproterozoic carbonates require a marine origin? A Pliocene- Pleistocene comparison. *Geology*, *40*(1), 87–90. https://doi.org/10.1130/G32538.1

Tucker, M. E. (1982). Precambrian dolomites: Petrographic and isotopic evidence that they differ from Phanerozoic dolomites. *Geology*, *10*(1), 7. https://doi.org/10.1130/0091-7613(1982)10<7:PDPAIE>2.0.CO;2

Urey, H. C. (1948). Oxygen isotopes in nature and in the laboratory. *Science*, *108*(2810), 489–496. Retrieved from. http://web.gps.caltech.edu/~tsai/files/GreatPapers/Urey_1948.pdf

Veizer, J., Ala, D., Azmy, K., Bruckschen, P., Buhl, D., Bruhn, F., et al. (1999). $^{87}Sr/^{86}Sr$, $\delta^{13}C$ and $\delta^{18}O$ evolution of Phanerozoic seawater. *Chemical Geology*, *161*(1-3), 59–88. https://doi.org/10.1016/S0009-2541(99)00081-9

Wenzel, B., Lécuyer, C., & Joachimski, M. M. (2000). Comparing oxygen isotope records of Silurian calcite and phosphate-$\delta^{18}O$ compositions of brachiopods and conodonts. *Geochimica et Cosmochimica Acta*, *64*(11), 1859–1872. https://doi.org/10.1016/S0016-7037(00)00337-9

Winkelstern, I. Z., & Lohmann, K. C. (2016). Shallow burial alteration of dolomite and limestone clumped isotope geochemistry. *Geology*, *44*(6), 467–470. https://doi.org/10.1130/G37809.1

Yang, J., Jansen, M. F., Macdonald, F. A., & Abbot, D. S. (2017). Persistence of a freshwater surface ocean after a snowball Earth. *Geology*, *45*(7), 615–618. https://doi.org/10.1130/G38920.1